Atmos. Chem. Phys., 14, 8343–8367, 2014
www.atmos-chem-phys.net/14/8343/2014/
doi:10.5194/acp-14-8343-2014

Atmospheric Chemistry and Physics
Open Access

Land-surface controls on afternoon precipitation diagnosed from observational data: uncertainties and confounding factors

B. P. Guillod[1], B. Orlowsky[1], D. Miralles[2,3], A. J. Teuling[4], P. D. Blanken[5], N. Buchmann[6], P. Ciais[7], M. Ek[8], K. L. Findell[9], P. Gentine[10], B. R. Lintner[11], R. L. Scott[12], B. Van den Hurk[13], and S. I. Seneviratne[1]

[1]ETH Zurich, Institute for Atmospheric and Climate Science, Zurich, Switzerland
[2]Ghent University, Laboratory of Hydrology and Water Management, Ghent, Belgium
[3]University of Bristol, School of Geographical Sciences, Bristol, UK
[4]Wageningen University, Hydrology and Quantitative Water Management Group, Wageningen, the Netherlands
[5]University of Colorado, Department of Geography, Boulder, CO, USA
[6]ETH Zurich, Institute of Agricultural Sciences, Zurich, Switzerland
[7]Laboratoire des Sciences du Climat et de l'Environnement, LSCE, Gif-sur-Yvette, France
[8]National Centers for Environmental Prediction, Suitland, MD, USA
[9]Geophysical Fluid Dynamics Laboratory, Princeton, NJ, USA
[10]Columbia University, Department of Earth and Environmental Engineering, New York, NY, USA
[11]Rutgers, The State University of New Jersey, Department of Environmental Sciences, New Brunswick, NJ, USA
[12]Southwest Watershed Research Center, USDA-ARS, Tucson, AZ, USA
[13]Royal Netherlands Meteorological Institute, KNMI, De Bilt, the Netherlands

Correspondence to: B. P. Guillod (benoit.guillod@env.ethz.ch) and S. I. Seneviratne (sonia.seneviratne@env.ethz.ch)

Received: 24 September 2013 – Published in Atmos. Chem. Phys. Discuss.: 7 November 2013
Revised: 2 July 2014 – Accepted: 3 July 2014 – Published: 20 August 2014

Abstract. The feedback between soil moisture and precipitation has long been a topic of interest due to its potential for improving weather and seasonal forecasts. The generally proposed mechanism assumes a control of soil moisture on precipitation via the partitioning of the surface turbulent heat fluxes, as assessed via the evaporative fraction (EF), i.e., the ratio of latent heat to the sum of latent and sensible heat, in particular under convective conditions. Our study investigates the poorly understood link between EF and precipitation by relating the before-noon EF to the frequency of afternoon precipitation over the contiguous US, through statistical analyses of multiple EF and precipitation data sets. We analyze remote-sensing data products (Global Land Evaporation: the Amsterdam Methodology (GLEAM) for EF, and radar precipitation from the NEXt generation weather RADar system (NEXRAD)), FLUXNET station data, and the North American Regional Reanalysis (NARR). Data sets agree on a region of positive relationship between EF and precipitation occurrence in the southwestern US. However, a region of strong positive relationship over the eastern US in NARR cannot be confirmed with observation-derived estimates (GLEAM, NEXRAD and FLUXNET). The GLEAM–NEXRAD data set combination indicates a region of positive EF–precipitation relationship in the central US. These disagreements emphasize large uncertainties in the EF data. Further analyses highlight that much of these EF–precipitation relationships could be explained by precipitation persistence alone, and it is unclear whether EF has an additional role in triggering afternoon precipitation. This also highlights the difficulties in isolating a land impact on precipitation. Regional analyses point to contrasting mechanisms over different regions. Over the eastern US, our analyses suggest that the EF–precipitation relationship in NARR is either atmospherically controlled (from precipitation persistence and potential evaporation) or driven by vegetation interception rather than soil moisture. Although this aligns well with the high forest cover and the wet regime of that region, the role of interception evaporation is likely overestimated because of low nighttime evaporation in NARR. Over the central and southwestern US, the EF–precipitation relationship is

additionally linked to soil moisture variations, owing to the soil-moisture-limited climate regime.

1 Introduction

Soil-moisture–precipitation feedback has been investigated for several decades and, despite some progress in recent years, remains a poorly understood process and a large source of uncertainty in climate models (Seneviratne et al., 2010). While studies until the 1990s tended to focus on the concept of moisture recycling (i.e., the fraction of precipitation directly contributed by regional evaporation from the land surface; see Seneviratne et al., 2010), more recent studies have emphasized the importance of indirect feedback mechanisms – that is, an influence of soil moisture on atmospheric stability, boundary layer characteristics, and thereby precipitation formation (e.g., Schär et al., 1999; Pal and Eltahir, 2001; Findell and Eltahir, 2003a; Ek and Holtslag, 2004; Betts, 2004; Santanello et al., 2009; Hohenegger et al., 2009; Taylor et al., 2011; Lintner et al., 2013; Gentine et al., 2013). Such indirect effects can theoretically lead to feedbacks of either sign (Seneviratne et al., 2010). For instance, over wet soils, humidity input into the boundary layer increases, but turbulence and boundary layer height decrease; the interplay of these two effects with the environment can trigger or suppress convective rainfall locally depending on the prevailing conditions (e.g., Ek and Holtslag, 2004; Gentine et al., 2013). Although most studies report a positive feedback, some suggest the existence of a negative feedback in certain regions (Findell and Eltahir, 2003a, b; Cook et al., 2006; Hohenegger et al., 2009; Westra et al., 2012; Gentine et al., 2013). Furthermore, nonlocal processes can also be important (e.g., Taylor and Ellis, 2006). In particular, spatial heterogeneity of soil moisture has been shown to possibly induce mesoscale circulations favoring precipitation over dry soils, for example in the Sahel region (Taylor et al., 2011) but also globally (Taylor et al., 2012).

The entire soil-moisture–precipitation feedback can be decomposed into a chain of processes as follows (Fig. 1, modified from Seneviratne et al., 2010; see also, e.g., Santanello et al., 2011):

A. Soil moisture impacts the partitioning of energy at the land surface into sensible and latent heat flux (H and λE, respectively), as quantified by the evaporative fraction $\mathrm{EF} = \frac{\lambda E}{H+\lambda E}$.

B. The moisture and heat input to the atmosphere corresponding to changes in EF impacts subsequent precipitation.

C. Precipitation impacts soil moisture by replenishing the soil moisture reservoir.

Relationship A (higher soil moisture leading to higher EF) is expected to be most significant in regions that are transitional between wet and dry climates, where soil moisture is the main limiting factor for land evaporation (e.g., Koster et al., 2004; Seneviratne et al., 2006b; Teuling et al., 2009; Hirschi et al., 2011). Note here the potentially negative feedback within relationship A (red arrow in Fig. 1), since increased soil moisture content enabling high evaporation leads to faster depletion of the soil moisture, thus dampening the initial evaporation increase (see also Seneviratne et al., 2010; Boé, 2013). Relationship B, i.e., higher EF leading to higher (or lower) precipitation, is generally the most uncertain part of the soil-moisture–precipitation coupling and feedback and can exhibit positive or negative sign through boundary layer regulation (e.g., Ek and Holtslag, 2004; Santanello et al., 2007; van Heerwaarden et al., 2009). The impact of precipitation on soil moisture (relationship C), on the other hand, can be considered as straightforward, albeit with a dependence on the partitioning of precipitation into interception, runoff, and infiltration. Some studies investigate single relationships (e.g., relationship A; see for instance Dirmeyer, 2011), while A–B has been analyzed as one relationship (e.g., Taylor et al., 2012) as well as by combining metrics from each individual relationship (A and B; e.g., Dirmeyer et al., 2012). The existence, the sign, and the strength of soil-moisture–precipitation coupling, i.e., the impact of soil moisture on precipitation (relationship A–B), and in particular EF–precipitation coupling (B), remain heavily debated in the literature.

Modeling studies yield contrasting results, identifying both positive (Schär et al., 1999; Pal and Eltahir, 2001; Koster et al., 2004) and negative soil-moisture–precipitation

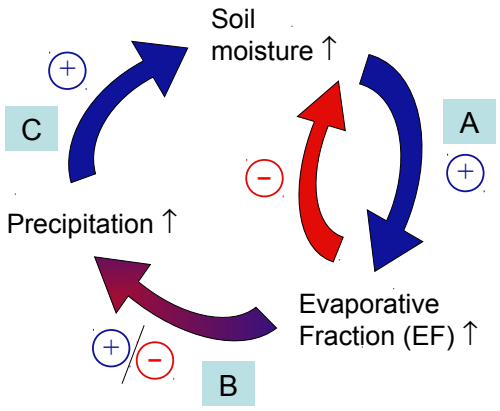

Figure 1. Schematic description of the soil-moisture–precipitation coupling and feedback loop. Positive arrows (blue) indicate processes leading to a positive soil-moisture–precipitation feedback (wetting for positive soil moisture anomaly, drying for negative soil moisture anomaly), the negative arrow (red) indicates a potential negative feedback damping the original soil moisture anomaly, and the red–blue arrow indicates the existence of both positive and negative feedbacks between evaporative fraction (EF) and precipitation anomalies. (A), (B), and (C) refer to the different steps of the feedback loop (see text). Modified from Seneviratne et al. (2010).

relationships in some cases (Findell and Eltahir, 2003a, b; Ek and Holtslag, 2004; Hohenegger et al., 2009; Siqueira et al., 2009; van den Hurk and van Meijgaard, 2010). It has been shown that model-based studies suffer from deficiencies, such as the dependence on the chosen convective parameterization or resolution (e.g., Hohenegger et al., 2009). In particular, Taylor et al. (2013) suggest that current convective parameterizations in models lead to a positive feedback in regions where observations and cloud-resolving simulations indicate negative feedback. Dirmeyer et al. (2006) highlight large biases in global climate models (GCMs) with respect to covariability between key atmospheric and land-surface variables, and Koster et al. (2003) suggest that soil-moisture–precipitation feedbacks may be overestimated in GCMs.

Given the large range of results from modeling studies, observational studies are necessary. However, for a number of reasons, these have been largely inconclusive (Seneviratne et al., 2010). First, the scarcity of soil moisture and EF measurements is a recurrent limitation. In particular, while recent satellite remote-sensing efforts have facilitated global analyses and generated new insights (e.g., Taylor et al., 2012), these only provide data of soil moisture in the top few millimeters of the soil and in regions without dense vegetation cover. This is often not representative of deeper layers and, thus, of EF, especially in vegetated areas. Second, we note that one of the most challenging tasks in assessing soil-moisture–precipitation coupling (i.e., A–B) from observational data is to establish causal rather than mere statistical links between soil moisture (or EF) and precipitation (see also Salvucci et al., 2002; Orlowsky and Seneviratne, 2010).

The difficulty of causal inferences from observational data arises from two main confounding effects. First, given the influence of precipitation on soil moisture (process C) it can be difficult to assess whether a detected relationship between soil moisture and precipitation is due to A–B, C, or both. In particular, persistence in precipitation at various timescales (from synoptic to interannual scales, including seasonal scale) can induce apparent causal links, for which even lagged correlations, such as between soil moisture and subsequent precipitation, may in fact simply reflect relationship C. Second, covariability between two variables (for instance soil moisture and convective precipitation) may be a necessary but not a sufficient condition for a causal link since it does not exclude the possibility that both quantities are governed by a third influencing variable (for instance sea surface temperature; see Orlowsky and Seneviratne, 2010). Ideally, potential confounding variables should be taken into account in observational analyses; this is, however, rarely done in practice, mostly due to difficulties in identifying confounding variables or lack of data availability.

In order to overcome the issue of data scarcity, some studies have used state-of-the-art reanalysis products (e.g., Bisselink and Dolman, 2008; Findell et al., 2011). Soil moisture and associated land-surface fluxes in reanalysis products are, however, ultimately model-based and therefore share the deficiencies of their land-surface models. Some reanalysis products assimilate screen-level variables (temperature, humidity) in order to better constrain the surface energy budget (Mahfouf, 1991; Bouttier et al., 1993a, b; Gentine et al., 2011) and may thus be advantageous over other reanalysis products. Nonetheless, such land data assimilation procedures may introduce biases in surface variables (e.g., Betts et al., 2003; Seneviratne et al., 2004). In addition, reanalyses suffer from other issues such as the lack of mass conservation. Finally, they suffer from the similar difficulties in isolating causal relationships as the studies based on observational data, although they provide a more comprehensive data basis. Therefore, reanalysis-based investigations are a useful complement to, but ultimately cannot replace, observational studies.

In this study, we investigate soil-moisture–EF–precipitation coupling (i.e., processes A and B, with a focus on B) over North America, addressing the aforementioned issues. We use direct observations of EF and precipitation from FLUXNET sites, remote-sensing-derived products (satellite-driven EF estimates from GLEAM and precipitation from the US radar network NEXRAD), and soil moisture, EF, and precipitation from the North American Regional Reanalysis, NARR (see Sect. 2). Specifically, we quantify the relationship between before-noon EF (and soil moisture) and afternoon convective rainfall occurrence via the triggering feedback strength (TFS; see Findell et al., 2011, and Sect. 3). This metric suggests, when applied to NARR, a region of positive coupling over the eastern US (Findell et al., 2011). Here, we first compare TFS estimates derived from observation-driven data sets with those from NARR (Sect. 4). We then consider the potentially confounding role of precipitation persistence on TFS (Sect. 5), and further investigate the role of soil moisture and vegetation interception storage on land evaporation, as well as the inferred EF–precipitation coupling (Sect. 6). Finally, results from these sections and their implications are discussed in Sect. 7.

2 Data sets

We provide here a description of the data sets used in this study. The analysis is restricted to North America for consistency with Findell et al. (2011). The data sets include a reanalysis product (the North American Regional Reanalysis, hereafter referred to as NARR), ground-based point-scale observations from FLUXNET, and remote-sensing-derived products: the NEXt generation weather RADar system (NEXRAD) and Global Land Evaporation: the Amsterdam Methodology (GLEAM). For 3-hourly data sets (NARR and GLEAM), the 3 h UTC time step closest to each local 3 h time period (in standard local time based on longitude) is

used, as in Findell et al. (2011). Thus, a lead or lag of up to 1 h may occur between the data sets.

2.1 NARR

The North American Regional Reanalysis (NARR; see Mesinger et al., 2006) is maintained at the National Center for Environmental Prediction (NCEP) and spans the period from 1979 to present. With its high spatial (about 32 km horizontal) and temporal (3 h) resolution, it allows for analyses focused on the diurnal evolution of land–atmosphere variables, which is an important aspect when analyzing the impact of surface fluxes on convection and precipitation. Its key characteristic is that it successfully assimilates high-quality precipitation observations into the atmospheric analysis, contrary to other reanalyses. This might in principle allow for a more realistic representation of land hydrology and land–atmosphere interactions. Humidity observations are also assimilated to constrain the atmospheric state, but they do not directly constrain surface fluxes via soil moisture nudging. Some other variables that affect the land surface, such as screen-level temperature, are not assimilated (Mesinger et al., 2006). Surface radiation fluxes can also be significantly biased in NARR (Kennedy et al., 2011). Moreover, West et al. (2007) identified spurious grid-scale precipitation events and related them to anomalous latent heating in cases of strong mismatch between assimilated and modeled precipitation. Ruane (2010a, b) highlighted that, while the exaggerated model precipitation is reduced by the assimilation of precipitation observations, other components of the water cycle such as evaporation and moisture convergence are not corrected. Indeed, assimilation products do not conserve water.

The land component of NARR is the Noah land-surface model (Ek et al., 2003). The soil includes four layers spanning the following depths: 0–10 cm, 10–40 cm, 40 cm–1 m, and 1–2 m. Bare soil evaporation (plant transpiration) is limited by soil moisture in the top layer (root zone), and evaporation from vegetation interception is accounted for. The root zone is defined for each grid cell as a function of vegetation type – at the analyzed sites, it includes the top three or four layers.

Here, we use NARR data from the years 1995–2007, and most of the analyses are restricted to days when data are available from other data sets (NEXRAD and GLEAM; see Sects. 2.3 and 2.4, respectively). This removes possible impacts of different time periods or time series lengths. Analyses of the longer 1979–2007 period are included in the Supplement (Sects. S1 and S4 in the Supplement) for comparison, yielding similar results.

All data are adjusted to local time by taking the 3 h period closest to the standard local time. Thus, for afternoon values, for instance, (12–6 p.m.), data from 09:00–15:00 UTC are used west from 247.5° E while 06:00–12:00 UTC data are used for the rest of the continent.

2.2 FLUXNET

FLUXNET is a global network of micrometeorological measurement sites (Baldocchi et al., 2001; Baldocchi, 2008), which uses the eddy-covariance technique to measure exchanges of CO_2, water, and energy between the land surface and the atmosphere. It currently includes over 500 sites worldwide (http://www.fluxnet.ornl.gov/introduction) with a relatively large density over Europe and North America. The density of the network as well as the record lengths in these regions allow for spatial analyses. FLUXNET is the largest available network of "direct" observations of latent and sensible heat fluxes, which, in spite of some known issues (underestimation of the fluxes and lack of energy balance closure, point-scale measurements with relatively small footprint area, possible change in footprint depending on, for example, wind direction), provides largely model-independent data and is therefore a direct estimate pertinent to our analyses.

In this study, we use data from the FLUXNET LaThuile data set, a global standardized database of eddy-covariance measurements which includes a large number of sites. Measurements of sensible (H) and latent (λE) heat fluxes are used to compute EF, while global radiation (i.e., incoming shortwave, R_g) and potential global radiation (i.e., extraterrestrial radiation, R_g^{pot}) are used to get a proxy for cloud cover (see Sect. 3.2). One of the main issues with eddy-covariance measurements is that the energy balance is not closed: the sum of H and λE typically underestimates the available energy by 10–30 % (e.g., Wilson et al., 2002; Mauder et al., 2006; Foken, 2008; Hendricks Franssen et al., 2010). However, as we do not use H and λE directly but only their ratio through EF, we note that the commonly used "fixed Bowen ratio" correction for the energy balance closure (i.e., attributing the missing energy to latent and sensible heat fluxes while keeping the Bowen ratio $B_w = \frac{H}{\lambda E}$ constant; e.g., Blanken et al., 1997) does not affect EF. Hence, we can expect that EF is only marginally affected by the lack of energy closure at the sites.

A total of 39 sites, listed in Table 1, are used in this study, all of them located in the US and Canada. The selection of the sites is based on several criteria: first, coverage by precipitation radars from NEXRAD (see Sect. 2.3) as well as R_g measurements are requirements for use in our study. Second, summers with many gaps in any of the required variables are removed, and only sites with a reasonable amount of remaining data are kept for the analysis ($\gtrsim$ 100 days).

2.3 NEXRAD

The NEXt generation weather RADar system (NEXRAD) is a network of 159 Weather Surveillance Radar-1988 Doppler (WSR-88D) sites covering the United States. Data are archived at the National Climatic Data Center (NCDC) of the US National Weather Service. Here, we use the 1 h

Table 1. FLUXNET sites included in this study, with latitude, longitude, altitude, vegetation class (IGBP, International Geosphere-Biosphere Programme), years available, years excluded from the analysis, and reference publication. IGBP classes represented in this subset of sites are croplands (CRO), closed shrublands (CSH), deciduous broadleaf forests (DBF), evergreen needleleaf forests (ENF), grasslands (GRA), mixed forests (MF), permanent wetlands (WET), and woody savannas (WSA). For a detailed description of the vegetation classes, see http://www.fluxdata.org/DataInfo/default.aspx/, accessed on 21 June 2013.

Site	Lat [° N]	Long [° E]	Altitude [m]	IGBP class	Years available	Years excluded	Reference
CA-Mer	45.41	−75.52	70	WET	1998–2005	2000	Roulet et al. (2007)
US-ARM	36.61	−97.49	314	CRO	2003–2006	–	Fischer et al. (2007)
US-Aud	31.59	−110.51	1469	GRA	2002–2006	–	Xiao et al. (2010)
US-Bkg	44.35	−96.84	510	GRA	2004–2006	–	Saito et al. (2009)
US-Blo	38.90	−120.63	1315	ENF	1997–2006	1997	Goldstein et al. (2000)
US-Bo1	40.01	−88.29	219	CRO	1996–2007	1996, 2007	Fisher et al. (2008)
US-Dk1	35.97	−79.09	168	GRA	2001–2005	–	Katul et al. (2003)
US-Dk3	35.98	−79.09	163	ENF	2001–2005	–	Johnson (1999)
US-FPe	48.31	−105.10	634	GRA	2000–2006	2001	Owen et al. (2007)
US-FR2	29.95	−97.00	271.9	WSA	2004–2006	–	Heinsch et al. (2004)
US-Goo	34.25	−89.87	87	GRA	2002–2006	2005	Yuan et al. (2007)
US-Ha1	42.54	−72.17	340	DBF	1991–2006	1991–1994, 1997, 2000–2005	Urbanski et al. (2007)
US-Ho1	45.20	−68.74	60	ENF	1996–2004	–	Fernandez et al. (1993)
US-Ho2	45.21	−68.75	91	ENF	1999–2004	–	Fernandez et al. (1993)
US-IB1	41.86	−88.22	225	CRO	2005–2007	–	Matamala et al. (2008)
US-IB2	41.84	−88.24	225	GRA	2004–2007	2004	Matamala et al. (2008)
US-KS2	28.61	−80.67	3	CSH	2000–2006	2003	Langley et al. (2002)
US-Los	46.08	−89.98	480	CSH	2001–2005	–	Yi et al. (2004)
US-LPH	42.54	−72.18	360–395	DBF	2002–2005	2005	Angert et al. (2003)
US-Me2	44.45	−121.56	1253	ENF	2003–2005	–	Thomas et al. (2009)
US-MMS	39.32	−86.41	275	DBF	1999–2005	1999, 2000	Pryor et al. (1999)
US-MOz	38.74	−92.20	219.4	DBF	2004–2006	–	Gu et al. (2007)
US-Ne3	41.18	−96.44	363	CRO	2001–2005	2005	Suyker et al. (2004)
US-PFa	45.95	−90.27	470	MF	1996–2003	1996	Mackay et al. (2002)
US-SO2	33.37	−116.62	1394	CSH	1997–2006	1997, 1998	Stylinski et al. (2002)
US-SO3	33.38	−116.62	1429	CSH	1997–2006	1998–2000, 2002–2004	Stylinski et al. (2002)
US-SP2	29.76	−82.24	50	ENF	1998–2004	1998, 1999	Bracho et al. (2011)
US-SP3	29.75	−82.16	50	ENF	1999–2004	1999	Bracho et al. (2011)
US-SRM	31.82	−110.87	1120	WSA	2004–2006	–	Scott et al. (2009)
US-Syv	46.24	−89.35	540	MF	2002–2006	2004	Desai et al. (2005)
US-Ton	38.43	−120.97	177	WSA	2001–2006	–	Ma et al. (2007)
US-UMB	45.56	−84.71	234	DBF	1999–2003	1999, 2002	Curtis et al. (2002)
US-Var	38.41	−120.95	129	GRA	2001–2006	2003, 2004	Ma et al. (2007)
US-WBW	35.96	−84.29	283	DBF	1995–1999	–	Greco and Baldocchi (1996)
US-WCr	45.81	−90.08	520	DBF	1999–2006	1999, 2004	Cook et al. (2004)
US-Wi4	46.74	−91.17	TBD	ENF	2002–2005	2003	Noormets et al. (2007)
US-Wkg	31.74	−109.94	1531	GRA	2004–2006	–	Scott et al. (2010)
US-Wrc	45.82	−121.95	371	ENF	1998–2006	2000, 2003, 2005, 2006	Waring and McDowell (2002)

precipitation product (N1P) from the level 3 data. More details about NEXRAD products can be found at http://www.ncdc.noaa.gov/oa/radar/radarresources.html (accessed on 20 December 2012). N1P data for summer (June to August, JJA) from 1995 to 2007 were downloaded at NEXRAD stations covering FLUXNET sites and their vicinity. We use 3 hr averages of precipitation within 20 km around each FLUXNET site. Aggregating with different radii and time-averaging methods leads to similar results (not shown).

2.4 GLEAM

GLEAM (Global Land Evaporation: the Amsterdam Methodology; see Miralles et al., 2011b) is a global data set of daily land-surface evaporation (E) based on satellite observations, available at a resolution of 0.25°. Estimates of E for day i are derived from

$$E_i = E_i^{\mathrm{pot}} S_i + (1-\beta) E_{I,i}, \quad (1)$$

Table 2. Data sets used in GLEAM product. Daily aggregates are computed locally to match the before-noon evaporative fraction (EF) estimate (i.e., starting and ending at around 9 a.m.; see Sect. 2.4). S and E^{pot} are the evaporative stress and the potential evaporation, respectively. See Sect. 2.4 for details.

Variables	Data set	Resolution and use
Soil moisture	NASA-LPRM (Owe et al., 2008) based on SSMI (1995–2002) and AMSR-E (from mid-2002)	nighttime overpass (for the S calculation)
Vegetation optical depth	NASA-LPRM (Owe et al., 2008)	daily (for the S calculation)
Precipitation	NEXRAD (Sect. 2.3)	daily (for the S calculation)
Net radiation	GEWEX SRB 3.0 (Stackhouse et al., 2004)	daily (for the S calculations) and 3-hourly frequencies (for the morning E^{pot})
Air temperature	NCEP-1 (Sheffield et al., 2006)	daily (for the S calculations) and 3-hourly frequencies (for the morning E^{pot})

where E_i^{pot} is the potential evaporation (at day i), derived through the Priestley and Taylor formulation (Priestley and Taylor, 1972) using data of net radiation (R^{net}) and near-surface air temperature. S_i denotes the evaporative stress (at day i) and is computed combining observations of vegetation water content (microwave vegetation optical depth) and estimates of root-zone soil moisture (θ_i) from a multilayer soil module driven by observations of precipitation (P_i) and surface soil moisture (θ_i^{obs}). The inclusion of vegetation optical depth accounts for the effects of plant phenology; its low day-to-day variability causes minor effects on the short-term dynamics of E_i. $E_{I,i}$ denotes the vegetation rainfall interception loss, calculated based on Gash's analytical model of rainfall interception (Gash, 1979) and described in Miralles et al. (2010); β is a constant to account for declines in transpiration when the canopy is wet (see Miralles et al., 2010, 2011b).

The satellite-data-driven evaporation model GLEAM is based on a larger array of satellite information than other evaporation products, which often apply algorithms requiring variables that are difficult to retrieve from satellite data (e.g., near-surface humidity and wind speed), and therefore rely on reanalysis forcing. To our knowledge, GLEAM is also the only large-scale satellite-data-driven evaporation product that estimates the temporal dynamics of root-zone soil moisture (based on observations of precipitation and surface soil moisture and a multilayer soil model). This root-zone soil moisture is used to constrain the atmospheric demand for water calculated based on radiation and temperature (note that explicit soil moisture constraints are not directly included in analogous models; e.g., Su, 2002; Mu et al., 2007; Fisher et al., 2008). GLEAM estimates of E have been extensively validated and compared to other methodologies (Miralles et al., 2011a, b; Mueller et al., 2013; Liu et al., 2013; Trambauer et al., 2014; Miralles et al., 2014a, b). In particular, GLEAM was successfully validated using measurements from 163 eddy-covariance stations and 701 soil moisture sensors all across the world and run with a wide range of data sets for the required input variables in Miralles et al. (2014b). λE estimates from GLEAM have been applied to a large number of studies over the past 3 years (e.g., Miralles et al., 2011a, 2012, 2014a, b; Reichle et al., 2011; Mueller et al., 2013; Liu et al., 2013; Fersch and Kunstmann, 2014; Jasechko et al., 2013; Trambauer et al., 2014), and the estimates error has been characterized using triple collocation (Miralles et al., 2011a).

We use a version of GLEAM that is driven by the input data sets noted in Table 2. Importantly, precipitation from NEXRAD (see Sect. 2.3) is used as input (to estimate interception loss and drive the soil module). GLEAM estimates using three other precipitation data sets yield similar results (Supplement S2, Fig. S3). GLEAM usually operates at daily time steps; as shown in Eq. (1), the computation of E_i requires daily estimates of potential evaporation, E_i^{pot}; evaporative stress, S_i; and interception, $E_{I,i}$. Here, to estimate before-noon EF (9 a.m.–12 p.m., i.e., $\mathrm{EF}_{i,9-12}$), several modifications to the original methodology are therefore necessary.

GLEAM is first run with daily input variables aggregated to days beginning/ending at around 9 a.m. standard local time. The resulting estimates of root-zone soil moisture (θ_{i-1}) used to derive S_{i-1} roughly correspond to 9 a.m. on day i, as they are derived using the cumulative precipitation up to 9 a.m. and instantaneous observations of surface soil moisture from the early morning hours (between 1.30 a.m. and 6 a.m. depending on the satellite platform – see Table 2 for details on the soil moisture remote-sensing products). In the assimilation, early morning surface soil moisture observations are combined with the bucket model estimates of soil moisture based on the rainfall until 9 a.m. Although surface

soil moisture might not always be representative of root-zone soil moisture, Miralles et al. (2014b) found mild improvements in the root-zone soil moisture estimates of GLEAM after assimilating the satellite observations.

Before-noon EF at day i (i.e., $\mathrm{EF}_{i,9-12}$) is then computed using S_{i-1} estimates as a proxy for the before-noon evaporative stress conditions. Since days with morning-time precipitation are not included in the computations of the TFS, $E_{I,i,9-12}$ is assumed to be zero. $\mathrm{EF}_{i,9-12}$ is therefore calculated as

$$\mathrm{EF}_{i,9-12} = \frac{\lambda E^{\mathrm{pot}}_{i,9-12} S_{i-1}}{R^{\mathrm{net}}_{i,9-12} - G_{i,9-12}}, \quad (2)$$

where R^{net} is net radiation from the GEWEX SRB data set (satellite-based product; see Stackhouse et al., 2004) and G is the ground heat flux, computed as a function of R^{net} and land cover type according to Miralles et al. (2011b). Note that the focus on the inter-day rather than intra-day variability in EF is advantageous since EF is considered most stable around noontime (e.g., Gentine et al., 2007). In addition, EF is rather robust to G given the low day-to-day variability in G relative to its diurnal cycle.

To summarize, $\mathrm{EF}_{i,9-12}$ is computed in two steps:

1. GLEAM is first run as in Miralles et al. (2011b) to derive the daily averages of evaporation (E_i) and evaporative stress (S_i) – see Eq. (1). The only difference here is that we compute daily values from about 9 a.m.–9 a.m. for all variables (depending on longitude but always before 9 a.m.).

2. S_{i-1} is used to calculate before-noon EF (i.e., $\mathrm{EF}_{i,9-12}$) using Eq. (2).

In this form, S_{i-1} accounts for evaporative stress due to soil moisture deficits only and does not account for interception. This is done to acknowledge that interception rates are high even at night (see e.g., Pearce et al., 1980) and therefore vegetation only remains wet for a few hours after rainfall (4 ± 1.9 h using values from field studies compiled by Miralles et al., 2010), and because days with morning rainfall are removed, not being the subject of our analyses (Sect. 3.2).

Nonetheless, to allow comparison with NARR, we introduce an alternative formulation which accounts for interception evaporation during the before-noon time period by assuming that vegetation stores intercepted water from the previous-day precipitation. To do so, we use a modified stress formulation, S^*_{i-1}, which assumes that water remains on vegetation from the previous-day precipitation. Hence, we can rearrange Eq. (1) as $E_i = E^{\mathrm{pot}}_i S_i + (1-\beta) E_{I,i} = E^{\mathrm{pot}}_i S^*_i$, which yields

$$S^*_{i-1} = S_{i-1} + (1-\beta)\frac{E_{I,i-1}}{E^{\mathrm{pot}}_{i-1}}. \quad (3)$$

Estimates of $\mathrm{EF}_{i,9-12}$ can then be computed using S^*_{i-1} instead of S_{i-1} in Eq. (2) to account for interception evaporation. Nonetheless, this alternative approach is likely unrealistic due to the above-mentioned fast evaporation rates. In addition, findings from field studies highlight that advection and downward sensible heat flux rather than radiation are critical to the evaporation of intercepted water (e.g., Pearce et al., 1980; Asdak et al., 1998; Holwerda et al., 2012), and therefore the contribution of interception evaporation to the (radiation-based) EF is not straightforward. Nonetheless, we use this alternative approach as a sensitivity test of potential interception effects in Sect. 6 (see Fig. 11).

Note that the timing of the input data sets for the S and S^* computation is crucial to this application, in particular for precipitation. First, we do not want to include any information about afternoon precipitation for the estimated before-noon EF on the same day. Second, rainfall occurring in the night preceding the estimated EF must be included in order to get an EF reflecting the conditions in the early morning. Unfortunately, the definition of "days" in many standard daily precipitation products varies, as shown in Table S1 in the Supplement, and is sometimes unclear: for instance, the use of data from the Global Precipitation Climatology Project (GPCP; see Huffman et al., 2001) is inappropriate due to the time window of the data set (00:00 to 00:00 UTC, i.e., from 4 p.m. (7 p.m.) to 4 p.m. (7 p.m.) in the US west (east) coast; see Table S1 in the Supplement). Also noteworthy, for the CPC Unified gauge product (Chen et al., 2008) days are defined differently depending on the country. For most of the US, the defined window is 12:00 to 12:00 (UTC, i.e., 4 a.m.–4 a.m. in the west coast/7 a.m.–7 a.m. in the east coast), which in principle suits our requirements, although uncertainties remain due to differing reporting times between contributing rain gauge stations. NEXRAD is not affected by this issue given its higher temporal resolution.

Due to the large diversity of precipitation products and the sensitivity of EF to precipitation, GLEAM has been driven with several precipitation data sets as input (see Supplement Discussion S2). Data sets used for this sensitivity test are NEXRAD, CPC Unified (Chen et al., 2008) and PERSIANN (Hsu et al., 1997). These three data sets either suit the required daily time window (like in the case of CPC Unified) or have a subdaily temporal resolution and therefore allow for appropriate daily aggregates (like in the case of NEXRAD and PERSIANN). Results obtained from these three independent precipitation data sets are qualitatively similar (see Fig. S3 and text in the Supplement).

3 Methods

This section describes the convection triggering metric TFS, including the selection of potentially convective days to which the computations are restricted, and the applied statistical test for assessing the significance of the results.

3.1 Triggering feedback strength (TFS)

The TFS, defined by Findell et al. (2011), quantifies the link between before-noon EF and afternoon precipitation occurrence as

$$\mathrm{TFS} = \sigma_{\mathrm{EF}} \frac{\partial \Gamma(r)}{\partial \mathrm{EF}}, \quad (4)$$

where EF is the before-noon evaporative fraction (computed between 9 a.m.–12 p.m., where 12 p.m. is noon), σ_{EF} is the standard deviation of EF and $\Gamma(r)$ is the probability of afternoon rain (> 1 mm, computed between 12 p.m. and 6 p.m.). The computation is restricted to summer days (June to August, JJA). Only potentially convective days (Sect. 3.2) are included in the computation in order to reduce the impact of large-scale synoptic systems. In addition, surface turbulent fluxes of sensible and latent heat are most likely to impact precipitation formation in convective situations (see Sect. 3.2). Note that, like most statistical analyses, a high TFS does not necessarily imply causality between EF and $\Gamma(r)$ but simply the existence of a statistical correlation between the two variables.

Findell et al. (2011) computed TFS in bins of the parameter space of EF, CTP, and $\mathrm{HI_{low}}$ (the convective triggering potential and a low-level humidity index, respectively; see Findell and Eltahir, 2003a), which are subsequently aggregated. $\mathrm{HI_{low}}$ is an indicator of humidity in the lower atmosphere, while CTP provides information about atmospheric stability. Accounting for these two variables is expected to reduce possible confounding effects from atmospheric conditions. In our study, however, relatively short observational time series preclude extensive sampling of this parameter space and independent observational sources for CTP and $\mathrm{HI_{low}}$, i.e., radio soundings, do not exist in the vicinity of all analyzed FLUXNET sites.

We can therefore only approximate the approach of Findell et al. (2011). Thus, we compute here a simplified version of TFS,

$$\mathrm{TFS}^* = \sigma_{\mathrm{EF}} \frac{\Gamma(r|\mathrm{EF} > \mathrm{EF_{Q60}}) - \Gamma(r|\mathrm{EF} \leq \mathrm{EF_{Q40}})}{\mathrm{EF_{Q80}} - \mathrm{EF_{Q20}}}, \quad (5)$$

where $\mathrm{EF_{QX}}$ is the Xth percentile of EF. The variable σ_{EF} and the percentiles of EF are determined for each location and data set independently. The definition of the bins ensures clearly distinct bins (i.e., no possible overlap even if $\mathrm{EF_{Q60}} = \mathrm{EF_{Q40}}$) while retaining most of the available data. Considering quantiles also partly accounts for different shapes of the EF distributions when comparing different EF data sets. EF values outside of the 0–1 range are excluded from the analysis. Although TFS^* is only an approximation of the original TFS defined by Findell et al. (2011), the two different computations show close agreement when applied to NARR.

3.2 Identification of potentially convective days

Midlatitude continental convection tends to occur in the afternoon, as a result of a particular daytime boundary layer evolution (Rio et al., 2009). Potentially convective days are therefore expected to be rain- and cloud-free in the morning. Moreover, convection is usually linked to low atmospheric stability and, therefore, typically positive CTP (Findell et al., 2011).

Findell et al. (2011) therefore identify potentially convective days as days with $\mathrm{CTP} > 0$ and no morning precipitation. In the absence of the necessary information for CTP from observations, we alternatively use the following criteria throughout our analyses:

- No morning precipitation, as in Findell et al. (2011), and
- $R_{\mathrm{g}}/R_{\mathrm{g}}^{\mathrm{pot}} > 0.67\max(R_{\mathrm{g}}/R_{\mathrm{g}}^{\mathrm{pot}})$ in the morning, where R_{g} is the global radiation (i.e., incoming shortwave) at the land surface and $R_{\mathrm{g}}^{\mathrm{pot}}$ is the potential R_{g} in the absence of atmosphere (i.e., extraterrestrial incoming shortwave).

R_{g} is available from NARR and measured at FLUXNET sites. $R_{\mathrm{g}}^{\mathrm{pot}}$, being dependent on time and latitude only, is computed for each grid cell used in our analysis for NARR. It is directly available in FLUXNET data. The computation of $\max(R_{\mathrm{g}}/R_{\mathrm{g}}^{\mathrm{pot}})$, restricted to summer days (JJA), is applied to each site to account for site-specific conditions. $R_{\mathrm{g}}/R_{\mathrm{g}}^{\mathrm{pot}}$ therefore quantifies the fraction of incoming solar radiation reaching the ground, and its maximum value corresponds to clear-sky cases. Requiring $R_{\mathrm{g}}/R_{\mathrm{g}}^{\mathrm{pot}} > 0.67\max(R_{\mathrm{g}}/R_{\mathrm{g}}^{\mathrm{pot}})$ in the morning is used to remove days with thick, persistent morning clouds from the analysis as they are likely linked to synoptic systems. Cutoff ratios between 0.5 and 0.8 do not lead to different results (not shown). Note that this criterion does not exclude the presence of morning clouds, which could be convective, but prevents cases dominated by morning clouds, likely of stratiform origin.

In this study, the data set combinations use these criteria computed on the following data sets, chosen according to data availability:

- NARR: precipitation and R_{g} from NARR,
- FLUXNET–NEXRAD: precipitation from NEXRAD and R_{g} from FLUXNET,
- GLEAM–NEXRAD: precipitation from NEXRAD and R_{g} from NARR.

The impact of the criteria for the selection of potentially convective days on TFS^*, in particular with respect to the NARR analysis and the different set of criteria used in our study compared to Findell et al. (2011), is small, as discussed in the Supplement (Sect. S1 and Fig. S2).

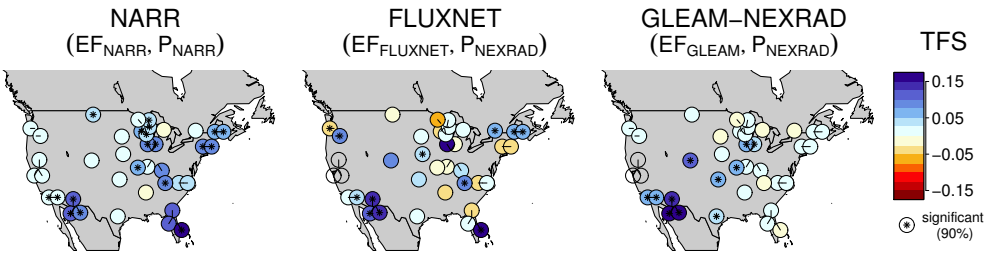

Figure 2. Triggering feedback strength (TFS*) in different data sets computed at FLUXNET sites. (left) Evaporative fraction (EF) and precipitation data from NARR, (center) EF from FLUXNET and precipitation from NEXRAD, and (right) EF from GLEAM and precipitation from NEXRAD. TFS* values significantly different from 0 at the 90 % level are indicated by a black asterisk. In case of overlap, points are shifted and the black lines inside the circles indicate the actual location of the station. Empty dots indicate sites with unreliable NEXRAD data.

3.3 Statistical tests

The statistical significance of TFS* $\neq 0$ is tested by bootstrap samples. A TFS* distribution is computed from 1000 bootstrap samples for which the EF data are kept unchanged and precipitation data are shuffled, which simulates the null hypothesis that no relation between EF and precipitation exists. The bootstrap TFS* distribution is approximately symmetrical with respect to 0. For a 90 % significance level, we require a positive (negative) TFS* to be at or above (below) the 95th percentile (5th percentile). We chose a rather low significance level of 90 % to account for the relatively short time series and the noise inherent in the data.

4 TFS from different data sets

The impact of before-noon EF on precipitation occurrence is quantified using the modified triggering feedback strength, TFS* (see Sect. 3). TFS* is computed at FLUXNET sites from three data set combinations: (i) a reanalysis product (NARR), (ii) direct measurements of surface turbulent heat fluxes at FLUXNET sites for EF in combination with radar precipitation from NEXRAD, and (iii) EF estimates from a satellite-data-driven evaporation product (GLEAM) in combination with NEXRAD precipitation. We compare estimates of TFS* from these data sets (Sect. 4.1) and general characteristics of the EF data sets (Sect. 4.2).

4.1 TFS patterns

Figure 2 displays TFS* for the three analyzed data set combinations. We note that the NARR pattern reproduces the regions of positive TFS* from Findell et al. (2011) over the eastern and southwestern US. This shows that our simplified TFS* computation (Eq. 5) reproduces the more sophisticated computation from Findell et al. (2011). Nonetheless, results from Fig. 2 (left) display slightly weaker and less significant values, shown in supplementary analyses to be a result of shorter time series (Fig. S1 in the Supplement). The impact of different sets of criteria for the selection of potentially convective days, another source of discrepancy between our analysis and Findell et al. (2011), turns out to be small (Fig. S2 in the Supplement).

To complement the maps shown in Fig. 2, the distribution of TFS* values for the three data sets are compared separately over three regions (western, central and eastern US) using box plots (Fig. 3). The definition of these regions is based on expected coupling regions from previous studies. The central US region represents an expected soil-moisture–precipitation coupling "hot spot" (e.g., Koster et al., 2004), while the eastern US displays a strong positive EF–precipitation relationship in NARR (Findell et al., 2011). The western US, on the other hand, is a dry region (soil-moisture-limited regime; see Thomas et al., 2009; Schwalm et al., 2012) with little soil moisture and EF variability and is therefore usually not considered conducive to strong soil-moisture–precipitation feedbacks. Strong EF–precipitation coupling is a necessary but not sufficient condition for strong soil-moisture–precipitation coupling.

Generally, FLUXNET displays large variations within each region (Fig. 3) and even within smaller climatic regions (e.g., in Florida, Fig. 2). It does not confirm the positive TFS* regional pattern evident in NARR over the eastern US (Fig. 2). The remote-sensing-derived estimate from GLEAM–NEXRAD displays more consistent patterns, but it also does not yield many significant positive TFS* values in that region (3 significant sites out of 23, Fig. 2). Over both the central US and southwestern US, GLEAM–NEXRAD and to some extent FLUXNET show larger TFS* values compared to NARR (Figs. 2 and 3). We note that inspection of the NEXRAD time series reveals suspect features (not shown) for three sites in the middle of the western region; results with NEXRAD (and GLEAM, which is partly based on NEXRAD) are therefore not shown for these sites (empty dots, e.g., in Fig. 3). Results at other sites have been confirmed by analyses with other precipitation data sets (not shown; e.g., with CMORPH; Joyce et al., 2004).

Several reasons might contribute to the observed differences between TFS* estimates from the different data sets, some of which can be discussed with the support of Fig. 4

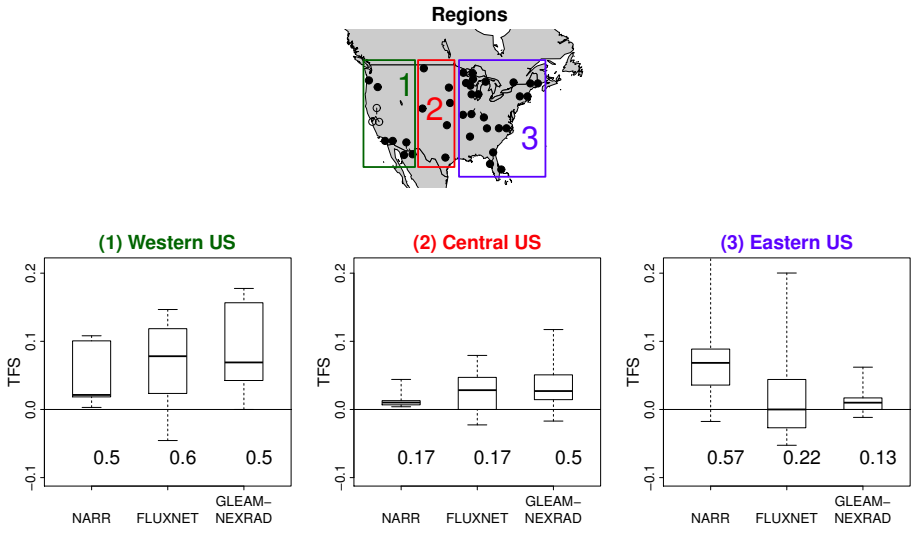

Figure 3. Quantitative comparison of the triggering feedback strength (TFS*) in different regions for the three data sets shown in Fig. 2. (top) Definition of the regions. (bottom) Box plot of TFS* in the three regions, where numbers below boxes indicate the fraction of sites with significant TFS*. Central lines denote medians, boxes show interquartile ranges, and whiskers denote minimum and maximum values. Empty dots on the map indicate sites with unreliable NEXRAD data and which are excluded from the box plot.

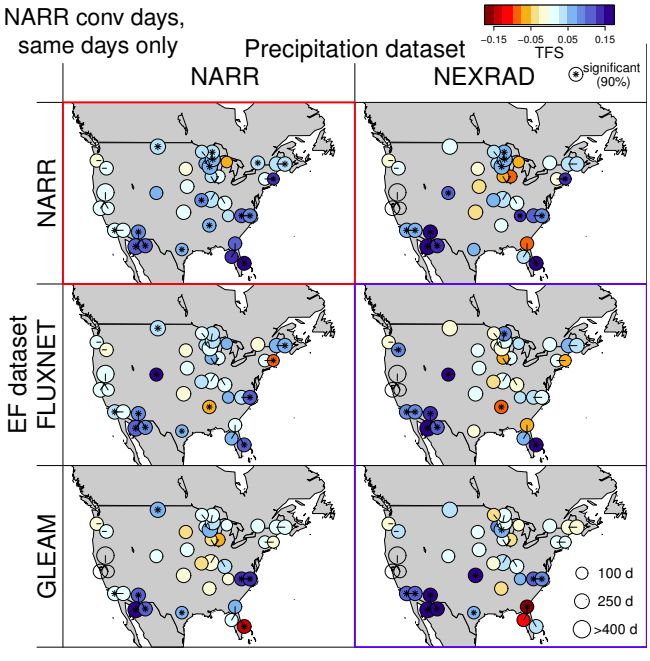

Figure 4. Influence of data set and sample size on TFS*. Only days with data in all data sets are included in the computation, and potentially convective days are further selected based on NARR (see Sect. 3.2). TFS* from NARR is boxed in red; TFS* from observation-based combinations in blue. The size of the dots indicates the number of days included in the computation according to the legend shown on the bottom right. TFS* values significantly different from 0 at the 90 % level are indicated by a black asterisk. Empty dots indicate sites with unreliable NEXRAD data.

(TFS* for the different combinations of EF and precipitation data sets for the same subset of days, namely the potentially convective days according to the NARR selection):

i. Spatial scale of the EF data: the footprint of FLUXNET measurements is much smaller than the grid cells of NARR and GLEAM (typically 100–2000 m and 25–30 km, respectively; see Sect. 4.2). Since EF–precipitation coupling is expected to occur at scales of about 20–100 km and NEXRAD data are at such a scale, FLUXNET may be less appropriate for this application. Although different TFS* cannot be clearly attributed to differences in footprints based on Fig. 4, EF uncertainties are shown to play a strong role in controlling the convection triggering metric (see also Sect. 4.2).

ii. Time series length and noise: the lengths of the time series considered here range from a few years in FLUXNET to 13 year (with some gaps) in GLEAM–NEXRAD and NARR. Comparing Fig. 2 with the respective panels of Fig. 4 shows that the decreased sample size in Fig. 4 affects TFS* in NARR and in the GLEAM–NEXRAD combination. A relatively large number of days is required to estimate TFS* robustly, as smaller or noisier samples lead to lower and less significant values. Thus, higher noise levels in observation-based data sets and incomplete sampling due to short record length could explain their weaker values of the metric in the eastern US.

iii. Selection of potentially convective days included in the TFS* computation (Sect. 3.2): the application of the criteria to different data sets potentially leads to different

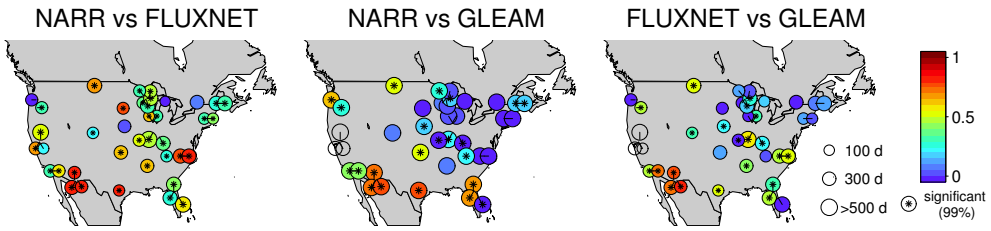

Figure 5. Correlation of daily JJA before-noon EF values between different data sets. The size of the dots indicates the number of days included in the computation according to the legend shown on the bottom right, and significant correlations at a 99 % level are indicated by a black asterisk. Empty dots for GLEAM indicate sites with unreliable NEXRAD (and thus GLEAM) data.

TFS* estimates, although sensitivity tests do not highlight a strong sensitivity of TFS* to the chosen criteria, as shown in the Supplement for NARR (Fig. S2).

iv. Other data set characteristics, such as temporal resolution, uncertainties, and possible errors (e.g., modeling components in NARR): such causes for the observed differences are difficult to disentangle from the three above-mentioned factors as the selection of days and the length of the time series are linked to the data sets. While the region of strong EF–precipitation relationship in the eastern US in NARR cannot be confirmed with FLUXNET and GLEAM–NEXRAD, it is possible that time series in these observation-derived data sets are simply too short or too noisy to detect a robust TFS* in this region. Nevertheless, NARR generally exhibits a stronger (weaker) link between EF and convection triggering over the eastern (central and southwestern) US compared to the observation-based estimates used here. Hence our results suggest a product dependence of the derived TFS* patterns.

Hereafter, we focus on the disentangling of these various factors, and in particular on possible fundamental differences in the processes underlying the investigated EF–precipitation relationship. Thereby, analysis of the differences in the data sets themselves might shed light on the different TFS* patterns. Since precipitation data from NARR and NEXRAD agree well in terms of precipitation occurrence (not shown), we focus on the differences between EF data sets and analyze these in the next section.

4.2 EF time series

To analyze the agreement of the spatiotemporal dynamics between the three EF data sets, Fig. 5 displays their respective correlations with one another in summer (JJA) for before-noon (9 a.m.–12 p.m.) EF. Unlike in the TFS* computation, all days are included in the correlations, but similar results are found for the potentially convective days only. Although positive, correlations are strikingly low at most sites and across all data set combinations. This suggests that the disagreement between the TFS* patterns in the different data set combinations is related to differences in the considered EF data sets (see also Fig. 4). Correlations of 10-day and monthly averages of before-noon EF are higher but remain low over the eastern US (Fig. S4 in the Supplement). Correlations of EF anomalies (i.e., after removing the seasonal cycle within JJA) instead of actual values display similar results (not shown).

Several reasons might explain these differences. First, the spatial scale over which EF is estimated, or footprint, is data-set-specific, as mentioned above (Sect. 4.1, point *i*). Differences might thus arise from contrasting environmental conditions over the respective footprints (e.g., input of water from rainfall in the case of very local precipitation events), but also from differences in land covers. Indeed, while wet vs. dry periods might be similar in all data sets, some studies have shown that different vegetation might respond differently to given conditions (Teuling et al., 2010). Land cover is in fact different at FLUXNET sites compared to the larger scale in NARR, in particular in regions with cultivated land, as FLUXNET sites are often located over natural vegetation. However, we did not find any systematic link between different land covers and resulting TFS* (not shown). Similarly, soil texture impacts soil moisture dynamics and EF (e.g., Guillod et al., 2013) and differences in local vs. larger scale soil texture could also be a reason for the differences in EF.

In order to better characterize the EF time series, Fig. 6 shows the mean, standard deviation, and persistence (quantified by the decorrelation timescale, τ_D, which integrates the autocorrelation function; see von Storch and Zwiers, 1999) for the three data sets. While we do not find any clear differences between the data sets that can explain the low temporal correlation and resulting differences in TFS*, the comparison highlights some interesting features. The mean EF is similar in all data sets and exhibits higher values in the eastern US (wetter climate) compared to the drier climate of the western US, although in GLEAM the central US displays even higher mean EF values. The EF standard deviation is noisy, although similar patterns are found across all data sets, with higher EF variability in the central US or in the Southern Great Plains (the exact location depending on the data set). Note, however, that the amplitudes differ widely among the three data sets. This does not necessarily impact TFS*: the

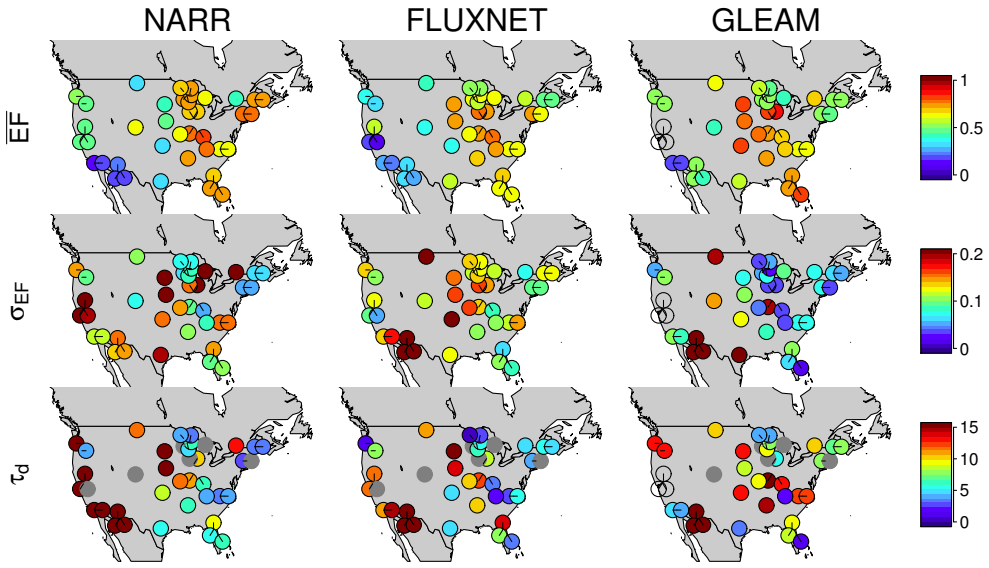

Figure 6. Statistical properties of EF data sets (NARR, FLUXNET, GLEAM, from left to right): (top) mean ($\overline{EF}$), (middle) standard deviation (σ_{EF}), and (bottom) decorrelation timescale (τ_d). Only days with data in all three data sets are included in the computation. The decorrelation timescale τ_d is computed following von Storch and Zwiers (1999). Grey dots indicate too many gaps for a reliable quantification of τ_d. Empty dots for GLEAM indicate sites with unreliable NEXRAD data.

change in the probability of afternoon precipitation with respect to EF is scaled by the standard deviation of EF (see Eq. 4 and Berg et al., 2013). Finally, EF persistence is generally lower in the eastern US, suggesting high variability at a scale of one to a few days in this region of strong relationship in NARR (Fig. 2, left). Thus, the regions of strong daily correlation between EF and convection triggering correspond, in NARR, to humid regions with low persistence, while in GLEAM–NEXRAD the drier southwestern region, with higher persistence, displays the strongest relationship. For the remaining analyses, we exclude FLUXNET data because of the record length of this data set being too limited.

5 Impact of EF vs. precipitation persistence

Although the TFS metric is a useful tool for investigating the relationship between EF and convective precipitation triggering, precipitation persistence might lead to high TFS even in the absence of an actual impact of EF on precipitation. Here, precipitation persistence refers to precipitation autocorrelation, which might be induced by atmospheric persistence (e.g., from synoptic weather patterns). Resulting persistent wet conditions cause higher EF and vice versa, potentially leading to high TFS* values simply through externally forced precipitation persistence. Although one cannot exclude the possibility that precipitation days cluster together due to a feedback mechanism, atmospheric forcing is a more likely reason. Precipitation persistence might also arise from seasonality in precipitation. However, this effect is less relevant for our study as only summer is considered, and analyses on individual months do not suggest a strong link to seasonality (not shown).

Ideally, the TFS computation should account for such confounding effects, via the filters for potentially convective days (see Sect. 3.2). In addition, Findell et al. (2011) use bins of CTP and HI_{low} in the computation, which we did not implement (Sect. 3.1). Nevertheless, we specifically test for the effect of day-to-day precipitation persistence on TFS* by replacing before-noon EF with precipitation from the previous day in the TFS* computation. With respect to an explanatory variable, X, we denote the change in the probability of afternoon precipitation for high vs. low X as $\Delta\Gamma(X) = \Gamma(r|X > X_{Q60}) - \Gamma(r|X \leq X_{Q40})$. Figure 7 (left) shows $\Delta\Gamma$(EF) for NARR and the GLEAM–NEXRAD combination, and the patterns strongly resemble those of TFS* (Fig. 2). Indeed, $\Delta\Gamma$(EF) is the term that controls most of the TFS* signal, since σ_{EF} and ∂EF mostly compensate each other in Eq. (4), and maps of σ_{EF} (Fig. 6) do not display a pattern similar to that of TFS* (Fig. 2). Using $\Delta\Gamma(X)$ allows for a direct comparison between the impact of EF and that of previous-day precipitation $P_{d,prev}$, shown on the right of Fig. 7 as $\Delta\Gamma(P_{d,prev})$. In fact, previous-day precipitation is a better predictor for afternoon precipitation occurrence than before-noon EF, which holds for both data sets and across all regions. Given these results, one can wonder whether the signal with EF is, in fact, only reflecting precipitation persistence or whether EF conveys additional information that can help explain afternoon precipitation.

In order to disentangle the impact of EF on precipitation from precipitation persistence, we apply a framework similar to Salvucci et al. (2002) to stratify the data based on

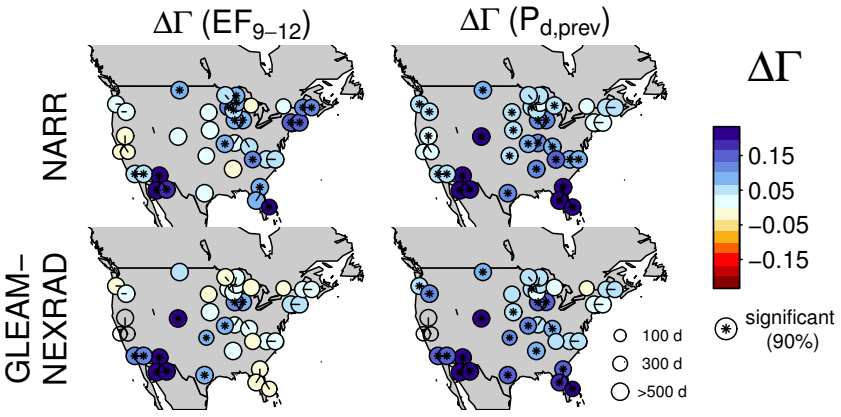

Figure 7. Difference in the probability of afternoon rainfall on days with high vs. low X, $\Delta\Gamma(X)$, where X is the before-noon EF (left panels) or previous-day precipitation (right panels), for NARR (top row) and GLEAM–NEXRAD (bottom row). High (low) X refers to values higher (lower) than the 60th (40th) percentile of X, i.e., $\Delta\Gamma(X) = \Gamma(r|X > X_{Q60}) - \Gamma(r|X \leq X_{Q40})$. Values significantly different from 0 at the 90 % level are indicated by a black asterisk. The size of the dots indicates the number of days included in the computation according to the legend shown on the bottom right map. Empty dots indicate sites with unreliable NEXRAD data.

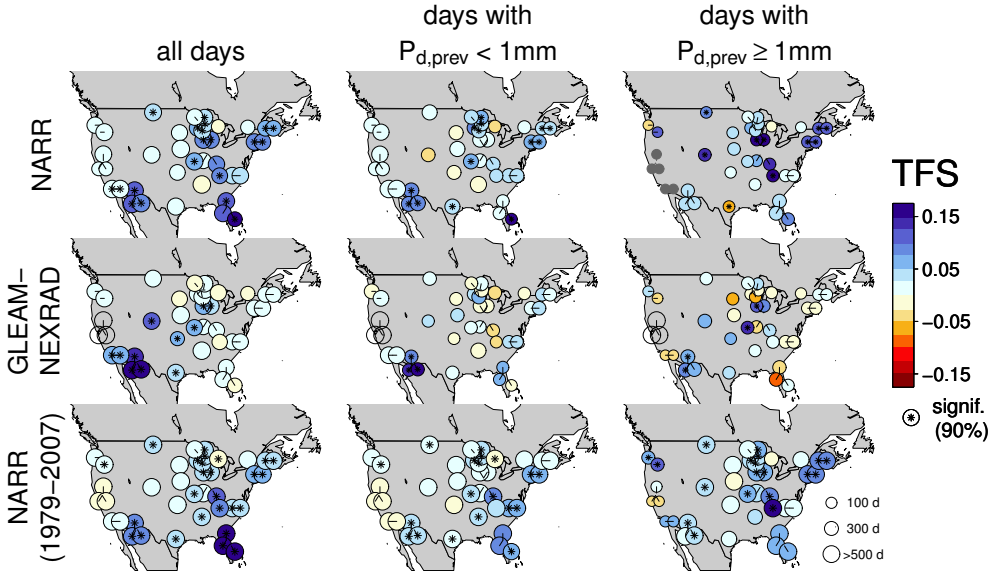

Figure 8. TFS* for subset of days: (left) all days and (center) days without and (right) days with rainfall on the previous day to account for precipitation persistence. Top row: NARR (years 1995–2007, as in the rest of the analysis). Middle row: GLEAM–NEXRAD combination. Bottom row: NARR, all years (1979–2007) for comparison, as the conditioning on previous-day precipitation reduces the number of days available for the computation. The size of the dots indicates the number of days included in the computation according to the legend shown on the bottom right map. Empty dots indicate sites with unreliable NEXRAD data.

previous-day precipitation. Here, only the occurrence of precipitation is considered and we investigate whether the signal emerging with EF reflects previous-day precipitation occurrence alone and thus may be an artifact of precipitation persistence on a short timescale. Note that Salvucci et al. (2002) also accounted for seasonal-scale persistence, which we omit since our analysis is restricted to summer months and our main interest is on short-term persistence (e.g., due to frontal systems or a sequence of these). Figure 8 shows TFS* independent of previous-day precipitation (i.e., as shown before; left column) as well as conditioned on the occurrence of precipitation the day before: here TFS* is computed for subsets of days with either no precipitation on the previous day or with precipitation on the previous day (center and right columns, respectively). Since the conditioning reduces the number of days available, this analysis is applied to NARR and GLEAM–NEXRAD as well as to the longer set of NARR data, covering 1979–2007 (bottom row) for comparison.

For both NARR and the GLEAM–NEXRAD combination, the signal over the eastern US strongly weakens when days are conditioned on previous-day rainfall (Fig. 8). This suggests an important role of precipitation persistence on subsequent precipitation and thus on TFS*. Note, however, that the shorter length of the time series after filtering days based on previous-day precipitation might also impact the results: using all available years from NARR (1979–2007, bottom row), TFS* is less sensitive to the conditioning on the previous day's rainfall, where EF might provide information on afternoon precipitation that is additional to previous-day precipitation occurrence. Nonetheless, for days following rain-free days, the weakening of the signal suggests a relevant role of precipitation persistence. Over the southwestern US, the signal appears less sensitive to day-to-day precipitation persistence as TFS* remains significant at most sites for both data sets.

Overall, precipitation persistence plays an important role and thereby affects TFS* in all data sets. Several factors can lead to high precipitation persistence via the atmosphere, such as atmospheric dynamics or SST forcing linked with large-scale teleconnection patterns. That said, we cannot exclude a partial contribution of EF–precipitation coupling to the identified persistence features, although larger $\Delta\Gamma$ with previous-day precipitation than with EF suggests that this is not the dominant mechanism. Finally, the binning in CTP and HI_{low} might already partly account for this effect in Findell et al. (2011).

6 Soil moisture and interception evaporation

In the conceptual framework of a feedback between soil moisture and precipitation via EF (Fig. 1), soil moisture is expected to be the main driver of EF. However, our analysis shows that EF can be highly variable from day to day (as reflected, for example, by the low autocorrelation in the eastern US; see Fig. 6). This feature is inconsistent with an impact of low-frequency soil moisture variations, which is generally the main relevant factor in the context of weather and seasonal forecasting (e.g., Koster and Suarez, 2001; Seneviratne et al., 2006a; Koster et al., 2010). We thus examine the relevance of soil moisture in the analyzed relationships between land conditions and convection triggering.

We recall that λE (and thereby EF) comprises three main components (Fig. 9): plant transpiration (E_{trans}), bare soil evaporation (E_{soil}), and evaporation of water intercepted by vegetation (E_I). These evaporate water from different reservoirs that typically evolve at different timescales. Root-zone soil moisture (W_{roots}), which reflects precipitation over the previous weeks to months and is affected by vegetation, provides a mid- to long-term storage for E_{trans}. Surface soil moisture (W_{top}, top few centimeters of the soil), which reflects precipitation over the preceding days or week, provides a short-term storage for E_{soil}. Finally, intercepted water on vegetation structures (W_{canopy}), which reflects precipitation over the preceding hours, provides very short storage for E_I. Although often neglected in climate studies, evaporation of intercepted rainfall has been estimated to represent more than 10 % of global terrestrial E (Miralles et al., 2011a) and 20–50 % over forests (e.g., Savenije, 2004; McLaren et al., 2008; Gerrits and Savenije, 2011). Typical timescales mentioned here reflect estimates from many studies (see, e.g., Salvucci and Entekhabi, 1994, for soil moisture or Scott et al., 1997, for individual components of evaporation) but may not encompass the entire range of possible interactions. Therefore, a feedback on precipitation through EF can, theoretically, result from any of the three components of λE (or a combination of them), all of them affected by antecedent precipitation itself.

As an extension to Fig. 1, Fig. 9 presents a schematic representation of the soil-moisture–precipitation feedback that distinguishes between the contributions of these three components of λE. Precipitation impacts the three storage terms on different timescales, which might then impact EF and, thereby, precipitation, forming three interlinked feedback loops. The first loop (C_1–A_1–B) acts on a short timescale through W_{canopy} and E_I, but is likely absent in our analysis due to the removal of days with morning rain. Indeed, field studies indicate high evaporation rates of intercepted water even at night (e.g., Pearce et al., 1980; Asdak et al., 1998; Holwerda et al., 2012), leading to complete evaporation of W_{canopy} within a few hours. Therefore, evening precipitation is unlikely to provide intercepted water available during the before-noon time period (transparent black–green arrow in Fig. 9). Morning rainfall, on the other hand, may provide before-noon W_{canopy} (black–green arrow) but given that such days may be of synoptic origin, they are excluded from our analysis, as noted previously. Moreover, in the few hours following rain, one may expect well-mixed conditions in the atmospheric boundary layer as well as low surface net radiation. Under these conditions, further rain would be more likely due to dynamical forcing from the atmosphere. The second loop (C_2–A_2–B) acts on a longer timescale, typically a few days, through W_{soil} and E_{soil}. Finally, a third loop (C_3–A_3–B) acts on a mid- to long timescale, typically weeks to months, via W_{roots} and E_{trans}. Ultimately, all three loops combine and act together on EF, which can impact precipitation. The distinction between these three components has, to our knowledge, rarely been discussed in the literature in the context of EF–precipitation coupling or soil-moisture–precipitation feedback (with exceptions, e.g., Savenije, 1995b, 2004, for moisture recycling and Scott et al., 1995, 1997, for precipitation persistence). However, they may help to better understand some of our results.

In order to investigate the role of these three components, we compute $\Delta\Gamma(X)$ using NARR data, where X is the water storage term controlling each component instead of EF. Storage terms are used instead of individual fluxes, since

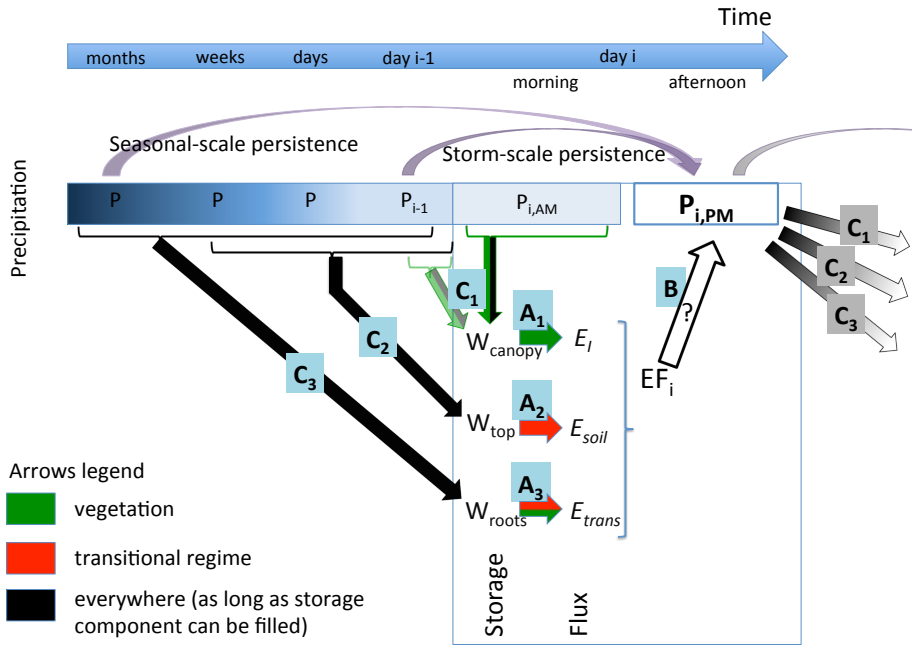

Figure 9. Different water storage components contributing to λE and their potential relevance for afternoon convective precipitation. The letters (A_i, B_i, C_i) refer to the steps of the feedback loop shown in Fig. 1, where "i" indicates the evaporation component of concern (1 for evaporation from vegetation interception, E_I; 2 for bare soil evaporation, E_{soil}; 3 for plant transpiration, E_{trans}). The horizontal axis represents time, ending with day i, and precipitation over the past days to months is represented with its persistence timescales and its typical influence on the three water storage terms shown below: canopy or vegetation interception storage W_{canopy} is affected by precipitation over the previous hours only (C_1). Surface soil moisture W_{top} is impacted by precipitation in the previous days to weeks (C_2). Root-zone soil moisture W_{roots} is mainly impacted by precipitation in the previous weeks to months (C_3). These three storages control their respective evaporation components, and thus EF, in different regions. Over vegetated areas for interception (A_1), in a transitional soil-moisture–climate regime for soil evaporation (A_2), and in regions which are both vegetated and in a transitional climate regime for transpiration (A_3). Note that A_2 and A_3 can also occur in other regions in some circumstances (e.g., over wet regions, during dry years), and W_{roots} includes W_{top}. Note that for loop 1 (through interception), a coupling cannot be distinguished from storm-scale precipitation persistence as before-noon interception is only expected in the presence of morning rain, mainly reflecting precipitation of synoptic origin. Precipitation over the previous evening usually does not affect before-noon W_{canopy}, but a transparent arrow is shown for rare cases where this might happen. Step B of the feedback remains a single component as the three evaporation components combine and only the total heat fluxes and their partitioning matter to precipitation occurrence.

these are not available from NARR output. Figure 10a–d displays $\Delta\Gamma$ in NARR computed with (a) EF, (b) surface soil moisture (for E_{soil}), (c) root-zone soil moisture (for E_{trans}), and (d) vegetation interception storage (for E_I). All these variables represent before-noon (9 a.m.–12 p.m.) values. The definition of surface and root-zone soil moisture in NARR is provided in Sect. 2.1.

Over the eastern US, most of the $\Delta\Gamma$ signal found with EF does not appear to be related to soil moisture (neither for surface nor for root-zone soil moisture, except in Florida). This suggests that the EF variability is not driven by soil moisture variations in this region. On the other hand, $\Delta\Gamma$ computed with morning vegetation interception storage displays a strong signal, suggesting that most of the signal with EF is linked to interception evaporation. However, $\Delta\Gamma$(EF) is not strongly sensitive to the exclusion of days with vegetation interception storage (Fig. 10e, while Fig. 10f displays the difference to the computation including all days and is rather small), despite the substantial fraction of days they represent in NARR (15–35 %, Fig. 10g). Since the remaining signal (Fig. 10e) cannot be attributed to vegetation interception, it is likely either due to one of the remaining terms of evaporation or to atmospheric controls on EF through potential evaporation.

To test this hypothesis, the third row of Fig. 10 displays $\Delta\Gamma(X)$ computed on days without vegetation interception and where X is (h) surface soil moisture, (i) root-zone soil moisture, and (j) potential EF ($EF_{pot} = \lambda E_{pot}/(R_n - G)$, i.e., the EF that corresponds to potential evaporation from NARR, which is based on Penman–Monteith equation). Since results are noisy due to the low number of included days, Fig. S5 in the Supplement displays the same analysis for the whole NARR time period (1979–2007). For most of the eastern US, $\Delta\Gamma(EF_{pot})$ appears to best reproduce the signal with EF on Supplement Fig. S5, suggesting that atmospheric controls on EF (through EF_{pot}) at least partly induce the apparent

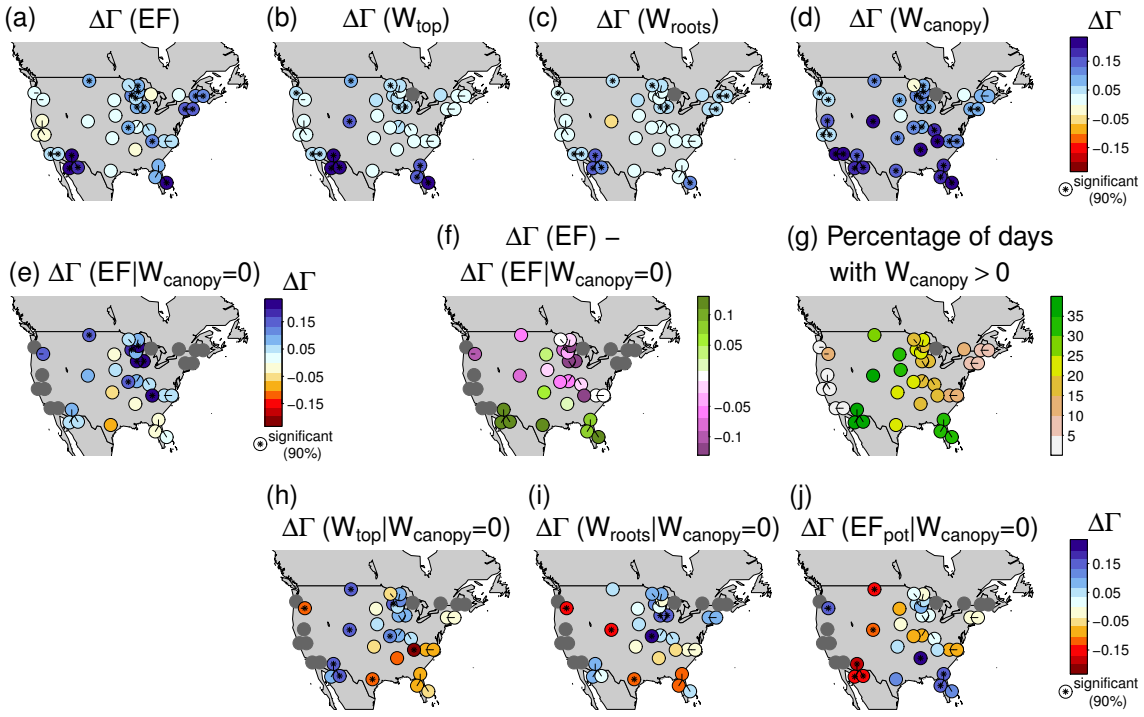

Figure 10. Identification of the drivers of the EF–precipitation relationship in NARR (see Supplement Fig. S5 for the same analysis using the longer NARR time period). Top row: difference in the probability of afternoon rainfall, $\Delta\Gamma(X)$ on days with high vs. low X, where X is the before-noon value of the different drivers. From left to right, X is **(a)** EF and **(b–d)** the three water storage terms that control EF: **(b)** surface soil moisture (W_{top}, controls bare soil evaporation), **(c)** root-zone soil moisture (W_{root}, controls plant transpiration), and **(d)** vegetation (canopy) interception storage (W_{canopy}, controls interception evaporation). Middle row: **(e)** $\Delta\Gamma(\mathrm{EF})$ computation restricted to days without canopy storage, **(f)** difference between $\Delta\Gamma(\mathrm{EF})$ computed with all days and with days without vegetation interception storage, and **(g)** percentage of days with interception storage. Bottom row: $\Delta\Gamma(X)$ restricted to days without interception storage, where X is **(h)** surface soil moisture, **(i)** root-zone soil moisture, and **(j)** potential EF ($\mathrm{EF_{pot}}$). High (low) X refers to values higher (lower) than the 60th (40th) percentile of X, i.e., $\Delta\Gamma(X) = \Gamma(r|X > X_{\mathrm{Q60}}) - \Gamma(r|X \leq X_{\mathrm{Q40}})$. Values significantly different from 0 at the 90 % level are indicated by a black asterisk. Grey dots indicate sites with no rainy days left.

positive coupling. Such a confounding effect could result from the control of temperature and humidity of the air mass on $\mathrm{EF_{pot}}$, which would then simply be a proxy for the likelihood of the air mass to produce rain, independently of surface fluxes.

Over other regions, we identify different key drivers based on Fig. 10 and Supplement Fig. S5. Over the southwestern US, our analysis highlights surface and root-zone soil moisture as important contributors, with interception playing a smaller role. Over the central US, no conclusion can be drawn from NARR as no EF–precipitation relationship is identified (see also Figs. 2 and 3).

As a sensitivity test, we also investigate the potential role of interception using GLEAM, where, in the default version, before-noon interception storage is neglected as it is based on a Gash analytical model (Gash, 1979), and therefore assumes that the vegetation water storage is evaporated within a model time step (Sect. 2.4). Here, we relax this assumption to allow comparison to results from NARR. Figure 11 displays TFS* for the GLEAM–NEXRAD combination as shown earlier (standard version, left) and including interception evaporation from previous-day precipitation (right; see Sect. 2.4 for details on the computation). Including interception in that way leads to an increase in significant positive TFS* signal, particularly over the eastern US, which is consistent with the results from NARR. However, we recall that this feature is likely not realistic: theoretical considerations do not support the presence of before-noon intercepted water storage in our analysis. Indeed, interception evaporation rates are high even at night (e.g., Pearce et al., 1980), as these are driven by advected energy or negative sensible heat flux rather than radiation (Pearce et al., 1980; Asdak et al., 1998; Holwerda et al., 2012). Thus, intercepted water evaporates within a few hours: for instance, a compilation of numerous studies on interception finds mean evaporation rates of $0.3 \pm 0.1\,\mathrm{mm\,h^{-1}}$ and canopy storage of $1.2 \pm 0.4\,\mathrm{mm}$, leading to complete evaporation of the whole canopy reservoir in $4 \pm 1.9\,\mathrm{h}$ (Miralles et al., 2010). The presence of interception storage during the before-noon time period is therefore largely restricted to days with morning precipitation, which

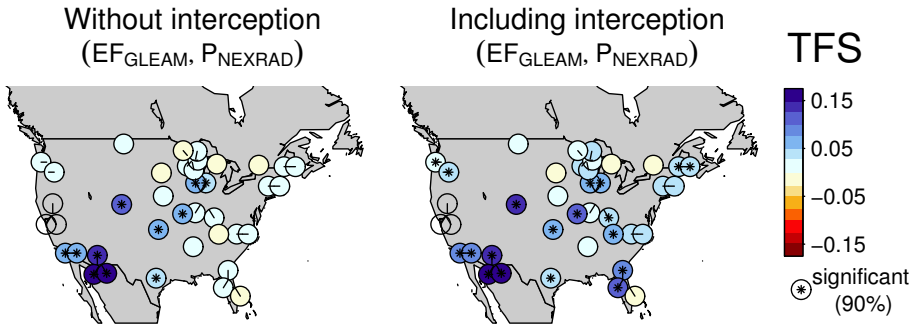

Figure 11. Influence of interception evaporation on TFS* in the GLEAM–NEXRAD combination. Left: interception is not included in the EF computation. Right: interception is included in the EF computation and EF is then capped at 1. Values significantly different from 0 at the 90 % level are indicated by a black asterisk. Empty dots indicate sites with unreliable NEXRAD data.

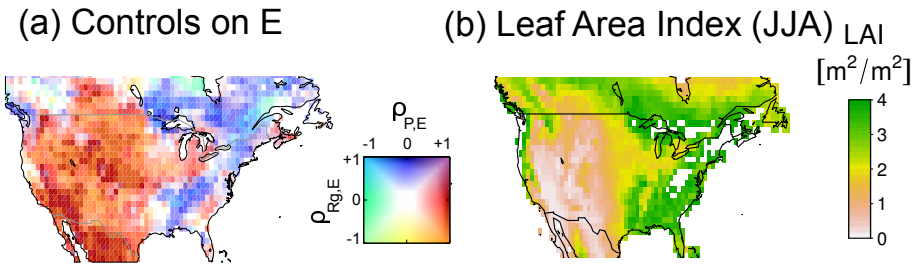

Figure 12. (a) Land evaporation regime (blue for wet regime, red for transitional regime): multi-model analysis of controls on yearly land evaporation from Teuling et al. (2009). Correlation between yearly evaporation and global radiation ($\rho_{R_g,E}$) and between yearly evaporation and precipitation ($\rho_{P,E}$), for the period 1986–1995. Each color corresponds to a unique combination of $\rho_{R_g,E}$ and $\rho_{P,E}$. **(b)** Mean summer (JJA) leaf area index [m^2 m^{-2}] over the period 1995–2007, from Stöckli et al. (2011).

are not included in our analysis as they are indicative of synoptic rainfall (Sect. 3.2). Some exceptions might occur under very humid nighttime atmospheric conditions, preventing intercepted water from evaporating, but these cases likely coincide with morning precipitation and are thus more likely to represent the dynamical forcing from the atmosphere.

Thus, these theoretical considerations based on past field studies suggest an overestimation of the impact of interception in NARR, in line with the results from the validation of other climate reanalysis and land-surface models (e.g., Reichle et al., 2011; Van den Hoof et al., 2013; Davies-Barnard et al., 2014). This could be due to the parameterization of interception as a function of E_{pot} (Chen et al., 1996), with interception unrealistically affected by net radiation (see Shuttleworth and Calder, 1979). Time series in NARR strongly support this hypothesis, showing that before-noon interception storage is most often provided by afternoon or evening precipitation on the previous day which does not evaporate in the night (see Supplement S5 and Fig. S6).

Overall, analyzing the role of individual components of λE in the relationship between EF and subsequent precipitation leads to similar conclusions in NARR and in GLEAM–NEXRAD. In the eastern US, vegetation interception evaporation and atmospheric controls on EF can lead to a likely overestimated relationship, due to, respectively, the fast rates of evaporation of intercepted water (see above) and the atmospheric origin of the signal. In the central and southwestern US, soil moisture (surface and root zone) drives the relationship where it exists, which would be consistent with the existence of a positive soil-moisture–precipitation feedback. These findings fit well with expectations based on climate regimes and vegetation cover: Fig. 12a highlights a wet regime in the eastern US, where land evaporation is controlled by radiation rather than soil moisture, unlike the soil-moisture–limited regime of the central and western US. In addition, vegetation interception is likely more relevant in the eastern US than in the central and southwestern US, as indicated by a high leaf area index in Fig. 12b. Although we recall that the interception-related findings from NARR are not consistent with knowledge from field studies for the above-mentioned reasons, an impact of evening or nighttime interception evaporation via moisture recycling remains possible on longer timescales.

7 Discussion and conclusions

A recent study (Findell et al., 2011) statistically relates the occurrence of afternoon convective precipitation to before-noon evaporative fraction (EF) through the TFS metric

(triggering feedback strength), based on data from the North American Regional Reanalysis (NARR), and suggests the existence of an extended region of positive land-surface–precipitation coupling over the eastern US. Our study extends that analysis with a systematic cross validation of additional, independent, observation-driven data sources and an in-depth investigation of all components contributing to the identified pattern from Findell et al. (2011).

Comparing the relationship patterns from the different data set combinations, the FLUXNET–NEXRAD and GLEAM–NEXRAD combinations do not reproduce positive TFS* in the eastern US found in NARR. Higher noise levels in these data sets and uneven sampling of different land cover types in the FLUXNET data may contribute to the differences. Nevertheless, our results suggest that land-surface dynamics in NARR and their stronger apparent coupling with precipitation in the eastern US might reflect model artifacts (see also Ferguson et al., 2012, who find that surface soil moisture from NARR correlates poorly with remote-sensing estimates in the eastern US). Conversely, a significant relationship between EF and convection triggering is found for the observation-driven GLEAM–NEXRAD combination in the central US (consistent with, e.g., Koster et al., 2004), although no such signal emerges from NARR in this region. The FLUXNET–NEXRAD combination displays low TFS* values there, possibly due to higher noise levels and short samples. Similarly, NARR might underestimate a possible EF–precipitation coupling in these regions. In the area of the southwestern US close to the Mexican border, all data sets agree on the existence of significant relationships between EF and convective triggering.

We find that the choice of the EF data set has a large impact on the relationship between EF and convection triggering, although the patterns of average EF, EF variability, and persistence in the different data sets do not clearly indicate the sources of this discrepancy. This comparison is further hampered by short observational records, uncertainties, and different spatial scales.

Furthermore, we find that precipitation of the previous day is a better predictor of afternoon precipitation than before-noon EF, pointing to a short timescale dominance of the atmosphere over land. Although EF seems to provide a small additional predictability to precipitation alone, the confounding effects of precipitation on EF via soil moisture or intercepted water precludes definite conclusions on the existence of a land–precipitation coupling at this stage. Accounting for the individual components of land evaporation (plant transpiration, bare soil evaporation, and evaporation of intercepted water) in the analysis, we find that the coupling, if present, arises from distinct sources in different regions.

Over the eastern US, atmospheric controls on EF (i.e., the atmospheric demand through potential evaporation) and vegetation interception drive the EF–precipitation relationship in NARR. Atmospheric controls on EF might induce an apparent relationship, but identifying these drivers as, for example, in Aires et al. (2013) lies beyond the scope of this study. The unrealistic presence of before-noon intercepted water from previous evening rainfall in NARR, likely due to an underestimation of the rates of evaporation of intercepted water at night, may falsely contribute to the positive TFS* over the eastern US, in line with the GLEAM–NEXRAD experiment (Fig. 11). This questions the reliability of NARR for these applications, despite its real advantage of high-quality precipitation assimilation. Other reanalysis products have issues with the representation of interception, e.g., MERRA (where the MERRA-Land product corrects for interception parameters among others; Reichle et al., 2011). These findings suggest a relatively short timescale of the EF–precipitation relationship in this region in NARR, which is consistent with the role of day-to-day precipitation persistence. Establishing a causal link between atmospheric- and interception-driven EF and precipitation is thus very difficult. Finally, we find that the EF–precipitation relationship found in NARR in the eastern US is not related to soil moisture, which makes sense given the humid climate regime with an expected low control of soil moisture on EF in this region, unlike what has been diagnosed in several studies for the central US (e.g., Koster et al., 2004; Teuling et al., 2009; Seneviratne et al., 2010).

The processes in central and southwestern US are, indeed, different from those in the eastern US. Wherever significant positive relationships between EF and precipitation occurrence are found in GLEAM–NEXRAD or NARR, soil moisture is identified as the primary driver. This is consistent with the soil-moisture-limited evaporation regime in this transitional region (Koster et al., 2004; Seneviratne et al., 2010; Mueller and Seneviratne, 2012) and aligns well with expected regions of soil-moisture–precipitation coupling (e.g., Koster et al., 2004).

A number of processes are not considered in our analysis, such as the dominance of orographic lifting over land–atmosphere interactions over the northwestern US where evaporation is soil-moisture-limited (e.g., Schwalm et al., 2012), the effects from different land covers (e.g., young vs. mature forests; see Vickers et al., 2012), or other processes acting at smaller scales than those considered here. Detailed analysis of these local features is, however, beyond the scope and spatial scale of our study.

A small part of the signal in the eastern US in NARR cannot be attributed to vegetation interception, soil moisture, and EF_{pot}. Nonlinear interactions between these variables possibly explain this signal, but the assimilation procedure may also affect it in a way that is difficult to assess. In GLEAM, the adjustments that were made to get estimates of before-noon EF introduce additional uncertainties that are difficult to quantify. Here we note that the reliability of the estimates is expected to decrease with increasing temporal resolution (Miralles et al., 2011b).

The presence of before-noon vegetation interception storage on days without morning precipitation is unlikely (based on previous field measurements, e.g., Pearce et al., 1980; Asdak et al., 1998; Holwerda et al., 2012). Thus, interception does not likely play a strong role for the triggering of convective storms via morning surface fluxes. Nonetheless, a direct impact via moisture recycling is possible and has already been suggested in the past (e.g., Savenije, 1995a, b). Additional moisture input to the atmosphere may thus provide more rainfall downwind on a longer timescale than the diurnal scale analyzed here. Indeed, evaporation from intercepted water has been estimated to amount to $\sim 11\,\%$ of global land evaporation (Miralles et al., 2011a) and to 20–50 % over forests (e.g., Savenije, 2004; McLaren et al., 2008; Gerrits and Savenije, 2011).

The discrepancies between the coupling patterns of precipitation with soil moisture and EF, respectively, as well as the here-proposed explanations through interception evaporation and atmospheric controls on EF, have hardly been addressed in the recent literature on land–precipitation coupling (e.g., Findell and Eltahir, 2003a; Seneviratne et al., 2010; Findell et al., 2011; Taylor et al., 2011; Ferguson et al., 2012; Taylor et al., 2012). This adds to the complexity of this coupling but possibly explains some of the contradictions from recent studies (e.g., Findell et al., 2011; Ferguson et al., 2012; Taylor et al., 2012). We show that not only the individual segments of the soil-moisture–precipitation coupling (Fig. 1; Wei and Dirmeyer, 2010; Dirmeyer, 2011), but also the individual components of λE may be crucial to uncover remaining uncertainties in land–atmosphere coupling.

Given the many unresolved issues in the investigation of land–precipitation coupling, further studies are required to pin down this complicated relationship. Analyses of the feedback accounting for precipitation persistence and confounding variables, applied to different temporal and spatial scales and a wide range of data sets, are urgently needed. Moreover, improvements in models would allow for more realistic sensitivity studies. Finally, soil moisture and EF observations at scales relevant to land–atmosphere coupling (i.e., 10 km) would provide invaluable observational constraints on model results and understanding of land–atmosphere coupling.

The Supplement related to this article is available online at doi:10.5194/acp-14-8343-2014-supplement.

Acknowledgements. We thank Han Dolman, Beverly E. Law, Altaf Alan, Markus Reichstein, Heini Wernli, and Christopher M. Taylor for discussions. We are also grateful for comments from the two anonymous reviewers. The authors acknowledge the Swiss State Secretariat for Education and Research SER for funding under the framework of the COST Action ES0804. NARR data is provided by the NOAA/OAR/ESRL PSD, Boulder, Colorado, USA, from their Web site at http://www.esrl.noaa.gov/psd/. This work used eddy-covariance data acquired by the FLUXNET community and in particular by the following networks: AmeriFlux (US Department of Energy, Biological and Environmental Research, Terrestrial Carbon Program – DE-FG02-04ER63917 and DE-FG02-04ER63911) and Fluxnet-Canada (supported by CFCAS, NSERC, BIOCAP, Environment Canada, and NRCan). We acknowledge the financial support of the eddy-covariance data harmonization provided by CarboEuropeIP, FAO-GTOS-TCO, iLEAPS, Max Planck Institute for Biogeochemistry, National Science Foundation, University of Tuscia, University Laval, Environment Canada, and US Department of Energy, and the database development and technical support from Berkeley Water Center, Lawrence Berkeley National Laboratory, Microsoft Research eScience, Oak Ridge National Laboratory, University of California – Berkeley, and the University of Virginia.

Edited by: L. Ganzeveld

References

Aires, F., Gentine, P., Findell, K. L., Lintner, B. R., and Kerr, C.: Neural Network-Based Sensitivity Analysis of Summertime Convection over the Continental United States, J. Climate, 27, 1958–1979, doi:10.1175/JCLI-D-13-00161.1, 2013.

Angert, A., Barkan, E., Barnett, B., Brugnoli, E., Davidson, E. A., Fessenden, J., Maneepong, S., Panapitukkul, N., Randerson, J. T., Savage, K., Yakir, D., and Luz, B.: Contribution of soil respiration in tropical, temperate, and boreal forests to the 18O enrichment of atmospheric O_2, Global Biogeochem. Cy., 17, 1089, doi:10.1029/2003GB002056, 2003.

Asdak, C., Jarvis, P. G., and Gardingen, P. V.: Evaporation of intercepted precipitation based on an energy balance in unlogged and logged forest areas of central Kalimantan, Indonesia , Agr. Forest Meteorol., 92, 173–180, doi:10.1016/S0168-1923(98)00097-5, 1998.

Baldocchi, D.: "Breathing" of the terrestrial biosphere: lessons learned from a global network of carbon dioxide flux measurement systems, Aust J. Bot., 56, 1–26, doi:10.1071/BT07151, 2008.

Baldocchi, D., Falge, E., Gu, L., Olson, R., Hollinger, D., Running, S., Anthoni, P., Bernhofer, C., Davis, K., Evans, R., Fuentes, J., Goldstein, A., Katul, G., Law, B., Lee, X., Malhi, Y., Meyers, T., Munger, W., Oechel, W., Paw, K. T., Pilegaard, K., Schmid, H. P., Valentini, R., Verma, S., Vesala, T., Wilson, K., and Wofsy, S.: FLUXNET: A New Tool to Study the Temporal and Spatial Variability of Ecosystem-Scale Carbon Dioxide, Water Vapor, and Energy Flux Densities, B. Am. Meteorol. Soc., 82, 2415–2434, doi:10.1175/1520-0477(2001)082<2415:FANTTS>2.3.CO;2, 2001.

Berg, A., Findell, K., Lintner, B. R., Gentine, P., and Kerr, C.: Precipitation Sensitivity to Surface Heat Fluxes over North America in Reanalysis and Model Data, J. Hydrometeorol., 14, 722–743, doi:10.1175/JHM-D-12-0111.1, 2013.

Betts, A. K.: Understanding Hydrometeorology Using Global Models, B. Am. Meteorol. Soc., 85, 1673–1688, doi:10.1175/BAMS-85-11-1673, 2004.

Betts, A. K., Ball, J. H., Bosilovich, M., Viterbo, P., Zhang, Y., and Rossow, W. B.: Intercomparison of water and energy budgets for

five Mississippi subbasins between ECMWF reanalysis (ERA-40) and NASA Data Assimilation Office fvGCM for 1990–1999, J. Geophys. Res., 108, 8618, doi:10.1029/2002JD003127, 2003.

Bisselink, B. and Dolman, A. J.: Precipitation Recycling: Moisture Sources over Europe using ERA-40 Data, J. Hydrometeorol., 9, 1073–1083, doi:10.1175/2008JHM962.1, 2008.

Blanken, P. D., Black, T. A., Yang, P. C., Neumann, H. H., Nesic, Z., Staebler, R., den Hartog, G., Novak, M. D., and Lee, X.: Energy balance and canopy conductance of a boreal aspen forest: Partitioning overstory and understory components, J. Geophys. Res., 102, 28915–28927, doi:10.1029/97JD00193, 1997.

Boé, J.: Modulation of soil moisture-precipitation interactions over France by large scale circulation, Clim. Dynam., 40, 875–892, doi:10.1007/s00382-012-1380-6, 2013.

Bouttier, F., Mahfouf, J.-F., and Noilhan, J.: Sequential Assimilation of Soil Moisture from Atmospheric Low-Level Parameters. Part II: Implementation in a Mesoscale Model, J. Appl. Meteorol., 32, 1352–1364, doi:10.1175/1520-0450(1993)032<1352:SAOSMF>2.0.CO;2, 1993a.

Bouttier, F., Mahfouf, J.-F., and Noilhan, J.: Sequential Assimilation of Soil Moisture from Atmospheric Low-Level Parameters. Part I: Sensitivity and Calibration Studies, J. Appl. Meteorol., 32, 1335–1351, doi:10.1175/1520-0450(1993)032<1335:SAOSMF>2.0.CO;2, 1993b.

Bracho, R., Starr, G., Gholz, H. L., Martin, T. A., Cropper, W. P., and Loescher, H. W.: Controls on carbon dynamics by ecosystem structure and climate for southeastern U.S. slash pine plantations, Ecol. Monogr., 82, 101–128, doi:10.1890/11-0587.1, 2011.

Chen, F., Mitchell, K., Schaake, J., Xue, Y., Pan, H.-L., Koren, V., Duan, Q. Y., Ek, M., and Betts, A.: Modeling of land surface evaporation by four schemes and comparison with FIFE observations, J. Geophys. Res., 101, 7251–7268, doi:10.1029/95JD02165, 1996.

Chen, M., Shi, W., Xie, P., Silva, V. B. S., Kousky, V. E., Wayne Higgins, R., and Janowiak, J. E.: Assessing objective techniques for gauge-based analyses of global daily precipitation, J. Geophys. Res., 113, D04110, doi:10.1029/2007JD009132, 2008.

Cook, B. D., Davis, K. J., Wang, W., Desai, A., Berger, B. W., Teclaw, R. M., Martin, J. G., Bolstad, P. V., Bakwin, P. S., Yi, C., and Heilman, W.: Carbon exchange and venting anomalies in an upland deciduous forest in northern Wisconsin, USA, Agr. Forest Meteorol., 126, 271–295, doi:10.1016/j.agrformet.2004.06.008, 2004.

Cook, B. I., Bonan, G. B., and Levis, S.: Soil Moisture Feedbacks to Precipitation in Southern Africa, J. Climate, 19, 4198–4206, doi:10.1175/JCLI3856.1, 2006.

Curtis, P. S., Hanson, P. J., Bolstad, P., Barford, C., Randolph, J., Schmid, H., and Wilson, K. B.: Biometric and eddy-covariance based estimates of annual carbon storage in five eastern North American deciduous forests, Agr. Forest Meteorol., 113, 3–19, doi:10.1016/S0168-1923(02)00099-0, FLUXNET 2000 Synthesis, 2002.

Davies-Barnard, T., Valdes, P., Jones, C., and Singarayer, J.: Sensitivity of a coupled climate model to canopy interception capacity, Clim. Dynam., 42, 1715–1732, doi:10.1007/s00382-014-2100-1, 2014.

Desai, A. R., Bolstad, P. V., Cook, B. D., Davis, K. J., and Carey, E. V.: Comparing net ecosystem exchange of carbon dioxide between an old-growth and mature forest in the upper Midwest, USAEk, Agr. Forest Meteorol., 128, 33–55, doi:10.1016/j.agrformet.2004.09.005, 2005.

Dirmeyer, P. A.: The terrestrial segment of soil moisture-climate coupling, Geophys. Res. Lett., 38, 1–5, doi:10.1029/2011GL048268, 2011.

Dirmeyer, P. A., Koster, R. D., and Guo, Z.: Do Global Models Properly Represent the Feedback between Land and Atmosphere?, J. Hydrometeorol., 7, 1177–1198, doi:10.1175/JHM532.1, 2006.

Dirmeyer, P. A., Cash, B. A., Kinter, J. L., Stan, C., Jung, T., Marx, L., Towers, P., Wedi, N., Adams, J. M., Altshuler, E. L., Huang, B., Jin, E. K., and Manganello, J.: Evidence for Enhanced Land-Atmosphere Feedback in a Warming Climate, J. Hydrometeorol., 13, 981–995, doi:10.1175/JHM-D-11-0104.1, 2012.

Ek, M. B. and Holtslag, A. A. M.: Influence of Soil Moisture on Boundary Layer Cloud Development, J. Hydrometeorol., 5, 86–99, doi:10.1175/1525-7541(2004)005<0086:IOSMOB>2.0.CO;2, 2004.

Ek, M. B., Mitchell, K. E., Lin, Y., Rogers, E., Grunmann, P., Koren, V., Gayno, G., and Tarpley, J. D.: Implementation of Noah land surface model advances in the National Centers for Environmental Prediction operational mesoscale Eta model, J. Geophys. Res., 108, 8851, doi:10.1029/2002JD003296, 2003.

Ferguson, C. R., Wood, E. F., and Vinukollu, R. K.: A Global Intercomparison of Modeled and Observed Land-Atmosphere Coupling, J. Hydrometeorol., 13, 749–784, doi:10.1175/JHM-D-11-0119.1, 2012.

Fernandez, I. J., Rustad, L. E., and Lawrence, G. B.: Estimating total soil mass, nutrient content, and trace metals in soils under a low elevation spruce-fir forest, Can. J. Soil. Sci., 73, 317–328, doi:10.4141/cjss93-034, 1993.

Fersch, B. and Kunstmann, H.: Atmospheric and terrestrial water budgets: sensitivity and performance of configurations and global driving data for long term continental scale WRF simulations, Clim. Dynam., 42, 2367–2396, doi:10.1007/s00382-013-1915-5, 2014.

Findell, K. L. and Eltahir, E. A. B.: Atmospheric Controls on Soil Moisture-Boundary Layer Interactions. Part I: Framework Development, J. Hydrometeorol., 4, 552–569, doi:10.1175/1525-7541(2003)004<0552:ACOSML>2.0.CO;2, 2003a.

Findell, K. L. and Eltahir, E. A. B.: Atmospheric Controls on Soil Moisture-Boundary Layer Interactions. Part II: Feedbacks within the Continental United States, J. Hydrometeorol., 4, 570–583, doi:10.1175/1525-7541(2003)004<0570:ACOSML>2.0.CO;2, 2003b.

Findell, K. L., Gentine, P., Lintner, B. R., and Kerr, C.: Probability of afternoon precipitation in eastern United States and Mexico enhanced by high evaporation, Nat. Geosci., 4, 434–439, doi:10.1038/ngeo1174, 2011.

Fischer, M. L., Billesbach, D. P., Berry, J. A., Riley, W. J., and Torn, M. S.: Spatiotemporal Variations in Growing Season Exchanges of CO_2, H_2O, and Sensible Heat in Agricultural Fields of the Southern Great Plains, Earth Interact., 11, 1–21, doi:10.1175/EI231.1, 2007.

Fisher, J. B., TU, K. P., and Baldocchi, D. D.: Global estimates of the land–atmosphere water flux based on monthly AVHRR and ISLSCP-II data, validated at 16 FLUXNET sites, Remote Sens. Environ., 112, 901–919, doi:10.1016/j.rse.2007.06.025, 2008.

Foken, T.: The Energy Balance Closure Problem: An Overview, Ecol. Appl., 18, 1351–1367, doi:10.1890/06-0922.1, 2008.

Gash, J. H. C.: An analytical model of rainfall interception by forests, Q. J. Roy. Meteor. Soc., 105, 43–55, doi:10.1002/qj.49710544304, 1979.

Gentine, P., Entekhabi, D., Chehbouni, A., Boulet, G., and Duchemin, B.: Analysis of evaporative fraction diurnal behaviour, Agr. Forest. Meteorol., 143, 13–29, doi:10.1016/j.agrformet.2006.11.002, 2007.

Gentine, P., Polcher, J., and Entekhabi, D.: Harmonic propagation of variability in surface energy balance within a coupled soil-vegetation-atmosphere system, Water Resour. Res., 47, 1–21, doi:10.1029/2010WR009268, 2011.

Gentine, P., Holtslag, A. A. M., D'Andrea, F., and Ek, M.: Surface and Atmospheric Controls on the Onset of Moist Convection over Land, J. Hydrometeorol., 14, 1443–1462, doi:10.1175/JHM-D-12-0137.1, 2013.

Gerrits, A. and Savenije, H.: 2.04 – Interception, in: Treatise on Water Science, edited by: Wilderer, P., pp. 89–101, Elsevier, Oxford, doi:10.1016/B978-0-444-53199-5.00029-4, 2011.

Goldstein, A., Hultman, N., Fracheboud, J., Bauer, M., Panek, J., Xu, M., Qi, Y., Guenther, A., and Baugh, W.: Effects of climate variability on the carbon dioxide, water, and sensible heat fluxes above a ponderosa pine plantation in the Sierra Nevada (CA), Agr. Forest Meteorol., 101, 113–129, doi:10.1016/S0168-1923(99)00168-9, 2000.

Greco, S. and Baldocchi, D. D.: Seasonal variations of CO_2 and water vapour exchange rates over a temperate deciduous forest, Glob. Change Biol., 2, 183–197, doi:10.1111/j.1365-2486.1996.tb00071.x, 1996.

Gu, L., Meyers, T., Pallardy, S. G., Hanson, P. J., Yang, B., Heuer, M., Hosman, K. P., Liu, Q., Riggs, J. S., Sluss, D., and Wullschleger, S. D.: Influences of biomass heat and biochemical energy storages on the land surface fluxes and radiative temperature, J. Geophys. Res., 112, D02107, doi:10.1029/2006JD007425, 2007.

Guillod, B. P., Davin, E. L., Kündig, C., Smiatek, G., and Seneviratne, S. I.: Impact of soil map specifications for European climate simulations, Clim. Dynam., 40, 123–141, doi:10.1007/s00382-012-1395-z, 2013.

Heinsch, F., Heilman, J., McInnes, K., Cobos, D., Zuberer, D., and Roelke, D.: Carbon dioxide exchange in a high marsh on the Texas Gulf Coast: effects of freshwater availability, Agr. Forest Meteorol., 125, 159–172, doi:10.1016/j.agrformet.2004.02.007, 2004.

Hendricks Franssen, H., Stöckli, R., Lehner, I., Rotenberg, E., and Seneviratne, S.: Energy balance closure of eddy-covariance data: A multisite analysis for European FLUXNET stations, Agr. Forest Meteorol., 150, 1553–1567, doi:10.1016/j.agrformet.2010.08.005, 2010.

Hirschi, M., Seneviratne, S. I., Alexandrov, V., Boberg, F., Boroneant, C., Christensen, O. B., Formayer, H., Orlowsky, B., and Stepanek, P.: Observational evidence for soil-moisture impact on hot extremes in southeastern Europe, Nat. Geosci., 4, 17–21, doi:10.1038/ngeo1032, 2011.

Hohenegger, C., Brockhaus, P., Bretherton, C. S., and Schär, C.: The Soil Moisture-Precipitation Feedback in Simulations with Explicit and Parameterized Convection, J. Climate, 22, 5003–5020, doi:10.1175/2009JCLI2604.1, 2009.

Holwerda, F., Bruijnzeel, L., Scatena, F., Vugts, H., and Meesters, A.: Wet canopy evaporation from a Puerto Rican lower montane rain forest: The importance of realistically estimated aerodynamic conductance, J. Hydrol., 414–415, 1–15, doi:10.1016/j.jhydrol.2011.07.033, 2012.

Hsu, K.-L., Gao, X., Sorooshian, S., and Gupta, H. V.: Precipitation Estimation from Remotely Sensed Information Using Artificial Neural Networks, J. Appl. Meteorol., 36, 1176–1190, doi:10.1175/1520-0450(1997)036<1176:PEFRSI>2.0.CO;2, 1997.

Huffman, G. J., Adler, R. F., Morrissey, M. M., Bolvin, D. T., Curtis, S., Joyce, R., McGavock, B., and Susskind, J.: Global Precipitation at One-Degree Daily Resolution from Multisatellite Observations, J. Hydrometeorol., 2, 36–50, doi:10.1175/1525-7541(2001)002<0036:GPAODD>2.0.CO;2, 2001.

Jasechko, S., Sharp, Z. D., Gibson, J. J., Birks, S. J., Yi, Y., and Fawcett, P. J.: Terrestrial water fluxes dominated by transpiration, Nature, 496, 347–350, doi:10.1038/nature11983, 2013.

Johnson, D. W.: Simulated nitrogen cycling response to elevated CO_2 in Pinus taeda and mixed deciduous forests, Tree Physiol., 19, 321–327, doi:10.1093/treephys/19.4-5.321, 1999.

Joyce, R. J., Janowiak, J. E., Arkin, P. A., and Xie, P.: CMORPH: A Method that Produces Global Precipitation Estimates from Passive Microwave and Infrared Data at High Spatial and Temporal Resolution, J. Hydrometeorol., 5, 487–503, doi:10.1175/1525-7541(2004)005<0487:CAMTPG>2.0.CO;2, 2004.

Katul, G., Leuning, R., and Oren, R.: Relationship between plant hydraulic and biochemical properties derived from a steady-state coupled water and carbon transport model, Plant Cell Environ., 26, 339–350, doi:10.1046/j.1365-3040.2003.00965.x, 2003.

Kennedy, A. D., Dong, X., Xi, B., Xie, S., Zhang, Y., and Chen, J.: A Comparison of MERRA and NARR Reanalyses with the DOE ARM SGP Data, J. Climate, 24, 4541–4557, doi:10.1175/2011JCLI3978.1, 2011.

Koster, R. D. and Suarez, M. J.: Soil Moisture Memory in Climate Models, J. Hydrometeorol., 2, 558–570, doi:10.1175/1525-7541(2001)002<0558:SMMICM>2.0.CO;2, 2001.

Koster, R. D., Suarez, M. J., Higgins, R. W., and Van den Dool, H. M.: Observational evidence that soil moisture variations affect precipitation, Geophys. Res. Lett., 30, 1–4, doi:10.1029/2002GL016571, 2003.

Koster, R. D., Dirmeyer, P. a., Guo, Z., Bonan, G., Chan, E., Cox, P., Gordon, C. T., Kanae, S., Kowalczyk, E., Lawrence, D., Liu, P., Lu, C.-H., Malyshev, S., McAvaney, B., Mitchell, K., Mocko, D., Oki, T., Oleson, K., Pitman, A., Sud, Y. C., Taylor, C. M., Verseghy, D., Vasic, R., Xue, Y., and Yamada, T.: Regions of strong coupling between soil moisture and precipitation, Science, 305, 1138–1140, doi:10.1126/science.1100217, 2004.

Koster, R. D., Mahanama, S. P. P., Yamada, T. J., Balsamo, G., Berg, A. A., Boisserie, M., Dirmeyer, P. A., Doblas-Reyes, F. J., Drewitt, G., Gordon, C. T., Guo, Z., Jeong, J.-H., Lawrence, D. M., Lee, W.-S., Li, Z., Luo, L., Malyshev, S., Merryfield, W. J., Seneviratne, S. I., Stanelle, T., van den Hurk, B. J. J. M., Vitart, F., and Wood, E. F.: Contribution of land surface initialization to subseasonal forecast skill: First results from a multi-model experiment, Geophys. Res. Lett., 37, 1–6, doi:10.1029/2009GL041677, 2010.

Langley, J., Drake, B., and Hungate, B.: Extensive belowground carbon storage supports roots and mycorrhizae in regenerating scrub

oaks, Oecologia, 131, 542–548, doi:10.1007/s00442-002-0932-6, 2002.

Lintner, B. R., Gentine, P., Findell, K. L., D'Andrea, F., Sobel, A. H., and Salvucci, G. D.: An Idealized Prototype for Large-Scale Land-Atmosphere Coupling, J. Climate, 26, 2379–2389, doi:10.1175/JCLI-D-11-00561.1, 2013.

Liu, Y., Zhuang, Q., Chen, M., Pan, Z., Tchebakova, N., Sokolov, A., Kicklighter, D., Melillo, J., Sirin, A., Zhou, G., He, Y., Chen, J., Bowling, L., Miralles, D., and Parfenova, E.: Response of evapotranspiration and water availability to changing climate and land cover on the Mongolian Plateau during the 21st century, Global Planet Change, 108, 85–99, doi:10.1016/j.gloplacha.2013.06.008, 2013.

Ma, S., Baldocchi, D. D., Xu, L., and Hehn, T.: Inter-annual variability in carbon dioxide exchange of an oak/grass savanna and open grassland in California, Agr. Forest Meteorol., 147, 157–171, doi:10.1016/j.agrformet.2007.07.008, 2007.

Mackay, D. S., Ahl, D. E., Ewers, B. E., Gower, S. T., Burrows, S. N., Samanta, S., and Davis, K. J.: Effects of aggregated classifications of forest composition on estimates of evapotranspiration in a northern Wisconsin forest, Glob. Change Biol., 8, 1253–1265, doi:10.1046/j.1365-2486.2002.00554.x, 2002.

Mahfouf, J.-F.: Analysis of Soil Moisture from Near-Surface Parameters: A Feasibility Study, J. Appl. Meteorol., 30, 1534–1547, doi:10.1175/1520-0450(1991)030<1534:AOSMFN>2.0.CO;2, 1991.

Matamala, R., Jastrow, J. D., Miller, R. M., and Garten, C. T.: Temporal Changes In C And N Stocks Of Restored Prairie: Implications For C Sequestration Strategies, Ecol. Appl., 18, 1470–1488, doi:10.1890/07-1609.1, 2008.

Mauder, M., Liebethal, C., Göckede, M., Leps, J.-P., Beyrich, F., and Foken, T.: Processing and quality control of flux data during LITFASS-2003, Bound.-Lay. Meteorol., 121, 67–88, doi:10.1007/s10546-006-9094-0, 2006.

McLaren, J. D., Arain, M. A., Khomik, M., Peichl, M., and Brodeur, J.: Water flux components and soil water-atmospheric controls in a temperate pine forest growing in a well-drained sandy soil, J. Geophys. Res., 113, G04031, doi:10.1029/2007JG000653, 2008.

Mesinger, F., DiMego, G., Kalnay, E., Mitchell, K., Shafran, P. C., Ebisuzaki, W., Jović, D., Woollen, J., Rogers, E., Berbery, E. H., Ek, M. B., Fan, Y., Grumbine, R., Higgins, W., Li, H., Lin, Y., Manikin, G., Parrish, D., and Shi, W.: North American Regional Reanalysis, B. Am. Meteorol. Soc., 87, 343–360, doi:10.1175/BAMS-87-3-343, 2006.

Miralles, D. G., Gash, J. H., Holmes, T. R. H., de Jeu, R. A. M., and Dolman, A. J.: Global canopy interception from satellite observations, J. Geophys. Res., 115, D16122, doi:10.1029/2009JD013530, 2010.

Miralles, D. G., De Jeu, R. A. M., Gash, J. H., Holmes, T. R. H., and Dolman, A. J.: Magnitude and variability of land evaporation and its components at the global scale, Hydrol. Earth Syst. Sci., 15, 967–981, doi:10.5194/hess-15-967-2011, 2011a.

Miralles, D. G., Holmes, T. R. H., De Jeu, R. A. M., Gash, J. H., Meesters, A. G. C. A., and Dolman, A. J.: Global land-surface evaporation estimated from satellite-based observations, Hydrol. Earth Syst. Sci., 15, 453–469, doi:10.5194/hess-15-453-2011, 2011b.

Miralles, D. G., van den Berg, M. J., Teuling, A. J., and de Jeu, R. A. M.: Soil moisture-temperature coupling: A multiscale observational analysis, Geophys. Res. Lett., 39, L21707, doi:10.1029/2012GL053703, 2012.

Miralles, D. G., Teuling, A. J., van Heerwaarden, C. C., and Vila-Guerau de Arellano, J.: Mega-heatwave temperatures due to combined soil desiccation and atmospheric heat accumulation, Nat. Geosci., 7, 345–349, doi:10.1038/ngeo2141, 2014a.

Miralles, D. G., van den Berg, M. J., Gash, J. H., Parinussa, R. M., de Jeu, R. A. M., Beck, H. E., Holmes, T. R. H., Jiménez, C., Verhoest, N. E. C., Dorigo, W. A., Teuling, A. J., and Johannes Dolman, A.: El Niño-La Niña cycle and recent trends in continental evaporation, Nat. Clim. Change, 4, 122–126, doi:10.1038/nclimate2068, 2014b.

Mu, Q., Heinsch, F. A., Zhao, M., and Running, S. W.: Development of a global evapotranspiration algorithm based on MODIS and global meteorology data, Remote Sens. Environ., 111, 519–536, doi:10.1016/j.rse.2007.04.015, 2007.

Mueller, B. and Seneviratne, S. I.: Hot days induced by precipitation deficits at the global scale, P. Natl. Acad. Sci. USA, 109, 12398–12403, doi:10.1073/pnas.1204330109, 2012.

Mueller, B., Hirschi, M., Jimenez, C., Ciais, P., Dirmeyer, P. A., Dolman, A. J., Fisher, J. B., Jung, M., Ludwig, F., Maignan, F., Miralles, D. G., McCabe, M. F., Reichstein, M., Sheffield, J., Wang, K., Wood, E. F., Zhang, Y., and Seneviratne, S. I.: Benchmark products for land evapotranspiration: LandFlux-EVAL multi-data set synthesis, Hydrol. Earth Syst. Sci., 17, 3707–3720, doi:10.5194/hess-17-3707-2013, 2013.

Noormets, A., Chen, J., and Crow, T.: Age-Dependent Changes in Ecosystem Carbon Fluxes in Managed Forests in Northern Wisconsin, USA, Ecosystems, 10, 187–203, doi:10.1007/s10021-007-9018-y, 2007.

Orlowsky, B. and Seneviratne, S. I.: Statistical Analyses of Land-Atmosphere Feedbacks and Their Possible Pitfalls, J. Climate, 23, 3918–3932, doi:10.1175/2010JCLI3366.1, 2010.

Owe, M., de Jeu, R., and Holmes, T.: Multisensor historical climatology of satellite-derived global land surface moisture, J. Geophys. Res., 113, F01002, doi:10.1029/2007JF000769, 2008.

Owen, K. E., Tenhunen, J., Reichstein, M., Wang, Q., Falge, E., Geyer, R., Xiao, X., Stoy, P., Ammann, C., Arain, A., Aubinet, M., Aurela, M., Bernhofer, C., Chojnicki, B. H., Granier, A., Gruenwald, T., Hadley, J., Heinesch, B., Hollinger, D., Knohl, A., Kutsch, W., Lohila, A., Meyers, T., Moors, E., Moureaux, C., Pilegaard, K., Saigusa, N., Verma, S., Vesala, T., and Vogel, C.: Linking flux network measurements to continental scale simulations: ecosystem carbon dioxide exchange capacity under non-water-stressed conditions, Glob. Change Biol., 13, 734–760, doi:10.1111/j.1365-2486.2007.01326.x, 2007.

Pal, J. S. and Eltahir, E. A. B.: Pathways Relating Soil Moisture Conditions to Future Summer Rainfall within a Model of the Land-Atmosphere System, J. Climate, 14, 1227–1242, doi:10.1175/1520-0442(2001)014<1227:PRSMCT>2.0.CO;2, 2001.

Pearce, A. J., Rowe, L. K., and Stewart, J. B.: Nighttime, wet canopy evaporation rates and the water balance of an evergreen mixed forest, Water Resour. Res., 16, 955–959, doi:10.1029/WR016i005p00955, 1980.

Priestley, C. H. B. and Taylor, R. J.: On the Assessment of Surface Heat Flux and Evaporation Using Large-Scale Parameters, Mon. Weather Rev., 100, 81–92, doi:10.1175/1520-0493(1972)100<0081:OTAOSH>2.3.CO;2, 1972.

Pryor, S. C., Barthelmie, R. J., and Jensen, B.: Nitrogen dry deposition at an AmeriFlux site in a hardwood forest in the midwest, Geophys. Res. Lett., 26, 691–694, doi:10.1029/1999GL900066, 1999.

Reichle, R. H., Koster, R. D., De Lannoy, G. J. M., Forman, B. A., Liu, Q., Mahanama, S. P. P., and Touré, A.: Assessment and Enhancement of MERRA Land Surface Hydrology Estimates, J. Climate, 24, 6322–6338, doi:10.1175/JCLI-D-10-05033.1, 2011.

Rio, C., Hourdin, F., Grandpeix, J.-Y., and Lafore, J.-P.: Shifting the diurnal cycle of parameterized deep convection over land, Geophys. Res. Lett., 36, L07809, doi:10.1029/2008GL036779, 2009.

Roulet, N. T., Lafleur, P. M., Richard, P. J. H., Moore, T. R., Humphreys, E. R., and Bubier, J.: Contemporary carbon balance and late Holocene carbon accumulation in a northern peatland, Glob. Change Biol., 13, 397–411, doi:10.1111/j.1365-2486.2006.01292.x, 2007.

Ruane, A. C.: NARR's Atmospheric Water Cycle Components. Part I: 20-Year Mean and Annual Interactions, J. Hydrometeorol., 11, 1205–1219, doi:10.1175/2010JHM1193.1, 2010a.

Ruane, A. C.: NARR's Atmospheric Water Cycle Components. Part II: Summertime Mean and Diurnal Interactions, J. Hydrometeorol., 11, 1220–1233, doi:10.1175/2010JHM1279.1, 2010b.

Saito, M., Maksyutov, S., Hirata, R., and Richardson, A. D.: An empirical model simulating diurnal and seasonal CO_2 flux for diverse vegetation types and climate conditions, Biogeosciences, 6, 585–599, doi:10.5194/bg-6-585-2009, 2009.

Salvucci, G. D. and Entekhabi, D.: Equivalent steady soil moisture profile and the time compression approximation in water balance modeling, Water Resour. Res., 30, 2737–2749, doi:10.1029/94WR00948, 1994.

Salvucci, G. D., Saleem, J. A., and Kaufmann, R.: Investigating soil moisture feedbacks on precipitation with tests of Granger causality, Adv. Water Res., 25, 1305–1312, doi:10.1016/S0309-1708(02)00057-X, 2002.

Santanello, J. A., Friedl, M. A., and Ek, M. B.: Convective Planetary Boundary Layer Interactions with the Land Surface at Diurnal Time Scales: Diagnostics and Feedbacks, J. Hydrometeorol., 8, 1082–1097, doi:10.1175/JHM614.1, 2007.

Santanello, J. A., Peters-Lidard, C. D., Kumar, S. V., Alonge, C., and Tao, W.-K.: A Modeling and Observational Framework for Diagnosing Local Land-Atmosphere Coupling on Diurnal Time Scales, J. Hydrometeorol., 10, 577–599, doi:10.1175/2009JHM1066.1, 2009.

Santanello, J. A., Peters-Lidard, C. D., and Kumar, S. V.: Diagnosing the Sensitivity of Local Land-Atmosphere Coupling via the Soil Moisture-Boundary Layer Interaction, J. Hydrometeorol., 12, 766–786, doi:10.1175/JHM-D-10-05014.1, 2011.

Savenije, H.: Does moisture feedback affect rainfall significantly?, Phys. Chem. Earth., 20, 507–513, doi:10.1016/S0079-1946(96)00014-6, 1995a.

Savenije, H. H.: New definitions for moisture recycling and the relationship with land-use changes in the Sahel, J. Hydrol., 167, 57–78, doi:10.1016/0022-1694(94)02632-L, 1995b.

Savenije, H. H. G.: The importance of interception and why we should delete the term evapotranspiration from our vocabulary, Hydrol. Process., 18, 1507–1511, doi:10.1002/hyp.5563, 2004.

Schär, C., Lüthi, D., Beyerle, U., and Heise, E.: The Soil-Precipitation Feedback: A Process Study with a Regional Climate Model, J. Climate, 12, 722–741, doi:10.1175/1520-0442(1999)012<0722:TSPFAP>2.0.CO;2, 1999.

Schwalm, C. R., Williams, C. A., Schaefer, K., Baldocchi, D., Black, T. A., Goldstein, A. H., Law, B. E., Oechel, W. C., Paw U, K. T., and Scott, R. L.: Reduction in carbon uptake during turn of the century drought in western North America, Nat. Geosci., 5, 551–556, doi:10.1038/ngeo1529, 2012.

Scott, R., Koster, R. D., Entekhabi, D., and Suarez, M. J.: Effect of a Canopy Interception Reservoir on Hydrological Persistence in a General Circulation Model, J. Climate, 8, 1917–1922, doi:10.1175/1520-0442(1995)008<1917:EOACIR>2.0.CO;2, 1995.

Scott, R., Entekhabi, D., Koster, R., and Suarez, M.: Timescales of Land Surface Evapotranspiration Response, J. Climate, 10, 559–566, doi:10.1175/1520-0442(1997)010<0559:TOLSER>2.0.CO;2, 1997.

Scott, R. L., Jenerette, G. D., Potts, D. L., and Huxman, T. E.: Effects of seasonal drought on net carbon dioxide exchange from a woody-plant-encroached semiarid grassland, J. Geophys. Res., 114, G04004, doi:10.1029/2008JG000900, 2009.

Scott, R. L., Hamerlynck, E. P., Jenerette, G. D., Moran, M. S., and Barron-Gafford, G. A.: Carbon dioxide exchange in a semidesert grassland through drought-induced vegetation change, J. Geophys. Res., 115, G03026, doi:10.1029/2010JG001348, 2010.

Seneviratne, S. I., Viterbo, P., Lüthi, D., and Schär, C.: Inferring Changes in Terrestrial Water Storage Using ERA-40 Reanalysis Data: The Mississippi River Basin, J. Climate, 17, 2039–2057, doi:10.1175/1520-0442(2004)017<2039:ICITWS>2.0.CO;2, 2004.

Seneviratne, S. I., Koster, R. D., Guo, Z., Dirmeyer, P. A., Kowalczyk, E., Lawrence, D., Liu, P., Mocko, D., Lu, C.-H., Oleson, K. W., and Verseghy, D.: Soil Moisture Memory in AGCM Simulations: Analysis of Global Land-Atmosphere Coupling Experiment (GLACE) Data, J. Hydrometeorol., 7, 1090–1112, doi:10.1175/JHM533.1, 2006a.

Seneviratne, S. I., Lüthi, D., Litschi, M., and Schär, C.: Land-atmosphere coupling and climate change in Europe, Nature, 443, 205–209, doi:10.1038/nature05095, 2006b.

Seneviratne, S. I., Corti, T., Davin, E. L., Hirschi, M., Jaeger, E. B., Lehner, I., Orlowsky, B., and Teuling, A. J.: Investigating soil moisture-climate interactions in a changing climate: A review, Earth. Sci. Rev., 99, 125–161, doi:10.1016/j.earscirev.2010.02.004, 2010.

Sheffield, J., Goteti, G., and Wood, E. F.: Development of a 50-Year High-Resolution Global Dataset of Meteorological Forcings for Land Surface Modeling, J. Climate, 19, 3088–3111, doi:10.1175/JCLI3790.1, 2006.

Shuttleworth, W. J. and Calder, I. R.: Has the Priestley-Taylor Equation Any Relevance to Forest Evaporation?, J. Appl. Meteorol., 18, 639–646, doi:10.1175/1520-0450(1979)018<0639:HTPTEA>2.0.CO;2, 1979.

Siqueira, M., Katul, G., and Porporato, A.: Soil Moisture Feedbacks on Convection Triggers: The Role of Soil-Plant Hydrodynamics, J. Hydrometeorol., 10, 96–112, doi:10.1175/2008JHM1027.1, 2009.

Stackhouse, P. W., Gupta, S. K., Cox, S. J., Mikovitz, J. C., Zhang, T., and Chiacchio, M.: 12 year surface radiation budget data set, GEWEX News, 14, 10–12, 2004.

Stöckli, R., Rutishauser, T., Baker, I., Liniger, M. A., and Denning, A. S.: A global reanalysis of vegetation phenology, J. Geophys. Res., 116, G03020, doi:10.1029/2010JG001545, 2011.

Stylinski, C., Gamon, J., and Oechel, W.: Seasonal patterns of reflectance indices, carotenoid pigments and photosynthesis of evergreen chaparral species, Oecologia, 131, 366–374, doi:10.1007/s00442-002-0905-9, 2002.

Su, Z.: The Surface Energy Balance System (SEBS) for estimation of turbulent heat fluxes, Hydrol. Earth Syst. Sci., 6, 85–100, doi:10.5194/hess-6-85-2002, 2002.

Suyker, A., Verma, S., Burba, G., Arkebauer, T., Walters, D., and Hubbard, K.: Growing season carbon dioxide exchange in irrigated and rainfed maize, Agr. Forest Meteorol., 124, 1–13, doi:10.1016/j.agrformet.2004.01.011, 2004.

Taylor, C. M. and Ellis, R. J.: Satellite detection of soil moisture impacts on convection at the mesoscale, Geophys. Res. Lett., 33, 11–14, doi:10.1029/2005GL025252, 2006.

Taylor, C. M., Gounou, A., Guichard, F., Harris, P. P., Ellis, R. J., Couvreux, F., and De Kauwe, M.: Frequency of Sahelian storm initiation enhanced over mesoscale soil-moisture patterns, Nat. Geosci., 4, 1–4, doi:10.1038/ngeo1173, 2011.

Taylor, C. M., de Jeu, R. A. M., Guichard, F., Harris, P. P., and Dorigo, W. A.: Afternoon rain more likely over drier soils, Nature, 489, 423–426, doi:10.1038/nature11377, 2012.

Taylor, C. M., Birch, C. E., Parker, D. J., Dixon, N., Guichard, F., Nikulin, G., and Lister, G. M. S.: Modeling soil moisture-precipitation feedback in the Sahel: Importance of spatial scale versus convective parameterization, Geophys. Res. Lett., 40, 6213–6218, doi:10.1002/2013GL058511, 2013.

Teuling, A. J., Hirschi, M., Ohmura, a., Wild, M., Reichstein, M., Ciais, P., Buchmann, N., Ammann, C., Montagnani, L., Richardson, A. D., Wohlfahrt, G., and Seneviratne, S. I.: A regional perspective on trends in continental evaporation, Geophys. Res. Lett., 36, 1–5, doi:10.1029/2008GL036584, 2009.

Teuling, A. J., Seneviratne, S. I., Stöckli, R., Reichstein, M., Moors, E., Ciais, P., Luyssaert, S., van den Hurk, B., Ammann, C., Bernhofer, C., Dellwik, E., Gianelle, D., Gielen, B., Grünwald, T., Klumpp, K., Montagnani, L., Moureaux, C., Sottocornola, M., and Wohlfahrt, G.: Contrasting response of European forest and grassland energy exchange to heatwaves, Nat. Geosci, 3, 722–727, doi:10.1038/ngeo950, 2010.

Thomas, C. K., Law, B. E., Irvine, J., Martin, J. G., Pettijohn, J. C., and Davis, K. J.: Seasonal hydrology explains interannual and seasonal variation in carbon and water exchange in a semiarid mature ponderosa pine forest in central Oregon, J. Geophys. Res., 114, G04006, doi:10.1029/2009JG001010, 2009.

Trambauer, P., Dutra, E., Maskey, S., Werner, M., Pappenberger, F., van Beek, L. P. H., and Uhlenbrook, S.: Comparison of different evaporation estimates over the African continent, Hydrol. Earth Syst. Sci., 18, 193–212, doi:10.5194/hess-18-193-2014, 2014.

Urbanski, S., Barford, C., Wofsy, S., Kucharik, C., Pyle, E., Budney, J., McKain, K., Fitzjarrald, D., Czikowsky, M., and Munger, J. W.: Factors controlling CO_2 exchange on timescales from hourly to decadal at Harvard Forest, J. Geophys. Res., 112, G02020, doi:10.1029/2006JG000293, 2007.

Van den Hoof, C., Vidale, P. L., Verhoef, A., and Vincke, C.: Improved evaporative flux partitioning and carbon flux in the land surface model JULES: Impact on the simulation of land surface processes in temperate Europe, Agr. Forest Meteorol., 181, 108–124, doi:10.1016/j.agrformet.2013.07.011, 2013.

van den Hurk, B. J. J. M. and van Meijgaard, E.: Diagnosing Land-Atmosphere Interaction from a Regional Climate Model Simulation over West Africa, J. Hydrometeorol., 11, 467–481, doi:10.1175/2009JHM1173.1, 2010.

van Heerwaarden, C. C., Vilà-Guerau de Arellano, J., Moene, A. F., and Holtslag, A. A. M.: Interactions between dry-air entrainment, surface evaporation and convective boundary-layer development, Q. J. Roy. Meteor. Soc., 135, 1277–1291, doi:10.1002/qj.431, 2009.

Vickers, D., Thomas, C. K., Pettijohn, C., Martin, J. G., and Law, B. E.: Five years of carbon fluxes and inherent water-use efficiency at two semi-arid pine forests with different disturbance histories, Tellus B, 64, 17159, doi:10.3402/tellusb.v64i0.17159, 2012.

von Storch, H. and Zwiers, F.: Statistical Analysis in Climate Research, Cambridge University Press, Cambridge, UK, 1999.

Waring, R. H. and McDowell, N.: Use of a physiological process model with forestry yield tables to set limits on annual carbon balances, Tree Physiol., 22, 179–188, doi:10.1093/treephys/22.2-3.179, 2002.

Wei, J. and Dirmeyer, P. A.: Toward understanding the large-scale land-atmosphere coupling in the models: Roles of different processes, Geophys. Res. Lett., 37, 1–5, doi:10.1029/2010GL044769, 2010.

West, G. L., Steenburgh, W. J., and Cheng, W. Y. Y.: Spurious Grid-Scale Precipitation in the North American Regional Reanalysis, Mon. Weather Rev., 135, 2168–2184, doi:10.1175/MWR3375.1, 2007.

Westra, D., Steeneveld, G. J., and Holtslag, A. A. M.: Some Observational Evidence for Dry Soils Supporting Enhanced Relative Humidity at the Convective Boundary Layer Top, J. Hydrometeorol., 13, 1347–1358, doi:10.1175/JHM-D-11-0136.1, 2012.

Wilson, K., Goldstein, A., Falge, E., Aubinet, M., Baldocchi, D., Berbigier, P., Bernhofer, C., Ceulemans, R., Dolman, H., Field, C., Grelle, A., Ibrom, A., Law, B., Kowalski, A., Meyers, T., Moncrieff, J., Monson, R., Oechel, W., Tenhunen, J., Valentini, R., and Verma, S.: Energy balance closure at FLUXNET sites, Agr. Forest Meteorol., 113, 223–243, doi:10.1016/S0168-1923(02)00109-0, FLUXNET 2000 Synthesis, 2002.

Xiao, J., Zhuang, Q., Law, B. E., Chen, J., Baldocchi, D. D., Cook, D. R., Oren, R., Richardson, A. D., Wharton, S., Ma, S., Martin, T. A., Verma, S. B., Suyker, A. E., Scott, R. L., Monson, R. K., Litvak, M., Hollinger, D. Y., Sun, G., Davis, K. J., Bolstad, P. V., Burns, S. P., Curtis, P. S., Drake, B. G., Falk, M., Fischer, M. L., Foster, D. R., Gu, L., Hadley, J. L., Katul, G. G., Matamala, R., McNulty, S., Meyers, T. P., Munger, J. W., Noormets, A., Oechel, W. C., U, K. T. P., Schmid, H. P., Starr, G., Torn, M. S., and Wofsy, S. C.: A continuous measure of gross primary production for the conterminous United States derived from MODIS and AmeriFlux data, Remote Sens. Environ., 114, 576–591, doi:10.1016/j.rse.2009.10.013, 2010.

Yi, C., Li, R., Bakwin, P. S., Desai, A., Ricciuto, D. M., Burns, S. P., Turnipseed, A. A., Wofsy, S. C., Munger, J. W., Wilson, K., and Monson, R. K.: A nonparametric method for separating photosynthesis and respiration components in CO_2 flux measurements, Geophys. Res. Lett., 31, L17107, doi:10.1029/2004GL020490, 2004.

Yuan, W., Liu, S., Zhou, G., Zhou, G., Tieszen, L. L., Baldocchi, D., Bernhofer, C., Gholz, H., Goldstein, A. H., Goulden, M. L., Hollinger, D. Y., Hu, Y., LAW, B. E., Stoy, P. C., Vesala, T., and Wofsy, S. C.: Deriving a light use efficiency model from eddy covariance flux data for predicting daily gross primary production across biomes, Agr. Forest Meteorol., 143, 189–207, doi:10.1016/j.agrformet.2006.12.001, 2007.